NASA Contractor Report 3379

An Airport Wind Shear Detection and Warning System Using Doppler Radar - A Feasibility Study

John McCarthy, Edward F. Blick,
and Kim L. Elmore

NASA

NASA Contractor Report 3379

An Airport Wind Shear Detection and Warning System Using Doppler Radar - A Feasibility Study

John McCarthy, Edward F. Blick,
and Kim L. Elmore
MCS, Inc.
Boulder, Colorado

NASA

National Aeronautics
and Space Administration

**Scientific and Technical
Information Branch**

1981

AUTHORS' ACKNOWLEDGEMENTS

TABLE OF CONTENTS

LIST OF TABLES

CHAPTER I

INTRODUCTION

During the past few years, both the aviation and atmospheric science communities have been examining the presence of severe wind shear situated along the approach or departure path of aircraft in the terminal environment. Numerous investigations have been made in an attempt to better understand the situations that can lead to serious aircraft accidents or incidents. Fujita and Caracena (1977), Frost and Crosby (1978), Frost and Reddy (1978), and McCarthy et al. (1979) have provided insight into conditions pertinent to accidents. Tinsley et al. (1978) has outlined the FAA's operational or planned solutions to the problem.

Fujita (1980) has documented seven accidents or incidents related to thunderstorm wind shear, the most recent of which was a near-accident of Eastern Air Lines Flight 693 at Atlanta Airport on August 22, 1979. Although the FAA has been examining and implementing solutions to the wind shear problem, the authors believe there is still room for improvement. Our work, and the work of Fujita (1980), indicate clearly that new systems must be developed to provide improved safety for civil air carriers.

In the last ten years, three basic concepts regarding adverse thunderstorm wind shear have emerged:

    a. <u>Gust Front</u>: The concept that thunderstorm outflow on a scale of 10 to 50 km horizontal extent is responsible for producing lethal wind shear for an aircraft. Goff (1976) presents this

case most clearly. Surface sensor techniques being implemented by the FAA address this feature with the Low-Level Wind Shear Alert System (LLWSAS) developed by Goff, and by a microbarograph system developed by Bedard et al. (1979); both are becoming operational at many major airports. Basically, a gust front, or other singular discontinuity, is sensed as surface wind or pressure change as it advects across an airport area; upon detection an alert is given automatically. The phenomenon is identified only as it is "reflected" in surface changes, and as a result these surface systems represent only "secondary" observing methods. Finally, the phenomenon measured is seen only on a scale ranging from 10 to 50 km, and does not appear to occur on a scale more closely tied to aircraft operations, such as 2 to 5 km.

b. Downburst. Fujita has proposed the existence of intense features in and near thunderstorms, that produce both down-drafts and horizontal outflows, on a scale of 3 to 5 km horizontally. An excellent description of this phenomenon is given in Fujita (1980). Of particular interest here is the fact that a downburst is of a rather small scale, one that fits well inside the approach or departure zone of an air-craft. In other words, this phenomenon is on the same length scale of an aircraft operating in the terminal area. This scale is in contrast to the gust front feature, which is characteristically of larger scale.

c. Phugoidal Waves. Groups represented by McCarthy and Frost have been examining the presence of rapidly varying horizontal

2

winds in the thunderstorm environment, and more specifically, calculating the response of aircraft to such winds. They found that long-period phugoidal response characteristics of high-performance jet transports could be excited by encounters with wave-like perturbations in horizontal wind, which, under certain conditions, result in major oscillations in altitude and airspeed, possibly leading to premature impact and/or stall. In their works, Frost and Crosby (1978), Frost and Reddy (1978), and McCarthy et al. (1979, 1980a, 1980b) found that the vertical component of the wind, as one of the consequences of Fujita's downburst, was relatively less important than was the horizontal, or headwind, component, and proposed the implementation of airborne systems designed to alert pilots of critical headwind/tailwind shear. Tinsley et al. (1978) and Foy (1979) best illustrate FAA concepts. In another FAA investigation of wind shear, Offi et al. (1980) describe a successful attempt to measure headwind along the approach path using an FAA ASR-8 surveillance radar. The work reported herein has been an application of the phugoidal response wind shear work of McCarthy et al. (1979) and of Frost and Crosby (1978) and Frost and Reddy (1978). We have recognized the importance of the longitudinal, or headwind/tailwind, component of wind in the thunderstorm environment as being most critical to aircraft performance. Although we accept the deleterious effect of the vertical, or downdraft, component, we have concentrated on the horizontal component because we believe that it can be readily detected. Real-time detection of the vertical component is much more difficult than real-time detection of the horizontal component.

3

We report on a feasibility study, conducted as part of SESAME '79 (an intensive research program designed to examine many aspects of severe thunderstorms). SESAME '79 was conducted near Norman, Oklahoma, between April 1, and June 15, 1979. Details can be found in SESAME (1978, 1979a, 1979b). Our objective was to examine the feasibility of measuring wind along a precision flight path, in the optically clear air, using a ground-based Doppler radar and, once these data were obtained, whether aircraft performance could be predicted using numerical simulation models. Two instru-mented wind measuring research aircraft were vectored along the approach path to verify the accuracy of the ground-based Doppler measurement and to verify numerical model-predicted performance characteristics. Three means of assessing performance were used, two relying on the air-speed ($\Delta u'$) and altitude ($\Delta h'$) approach deterioration parameters identified by McCarthy et al. (1979). The third method utilized quantitative pilot assessments of approach quality.

The overall objective of the study was to gauge the operational feasibility of a ground-based Doppler radar, operated in tandem with a computerized numerical simulation model of aircraft performance in the face of adverse wind shear to predict successfully dangerous situations for approaching and departing aircraft. In the sections to follow, we will describe the experimental plan in detail, discuss the measurement of winds along the approach path, using both Doppler and aircraft measurement systems, describe the application of the Blick[1] fixed stick simulation model, discuss the simulation model, discuss the pilot assessment tool, look at predicted versus actual aircraft performance, and, finally, discuss our overall assessment and recommended plans for future work.

[1]Professor of Aerospace Engineering, University of Oklahoma, Norman, Oklahoma.

4

CHAPTER II

EXPERIMENTAL PLAN

The following experimental tools were available and utilized in this study:

   a. A U.S. Air Force TPN-19 airport terminal area traffic control radar, a 10-cm wavelength surveillance radar, and a Precision Approach Radar (PAR) radar. The system was manned by air traffic controllers from FAA and the Air Force.

   b. A 10.2-cm pulsed Doppler radar located at the National Severe Storms Laboratory (NSSL), which could collect wind data in the optically clear air.

   c. A meteorologically instrumented Beech Queen Air aircraft and a similarly instrumented North American Sabreliner provided by the National Center for Atmospheric Research (NCAR). Both aircraft had an inertial navigation-based wind measurement system, capable of giving u, v and w gust components of the wind at high resolution, but we utilized only a 1 Hz resolution. Accuracies in the horizontal components are given as 1 m s^{-1}, while the accuracy in the vertical can be as high as 10 cm s^{-1}. From these measurements, the longitudinal (parallel to the aircraft axis of flight--or headwind-tailwind component) winds were derived. Additionally, altitude, true airspeed, pitch angle, INS position, along with many other parameters not used here, were recorded.

d. A numerical simulation model, developed by Blick, as reported in McCarthy et al. (1979), was used to predict performance of the two aircraft. The model included a fixed stick assumption (no pilot control or power changes were made); Frost and Turkel (1980) will report separately model results with utilized numerical pilot control functions.

Figure 1 is a map showing the horizontal placement of the approach paths, the runway, and the radar beam positions, used in this study. The radar was set to collect time series velocity data along a 3 deg elevation beam, which nearly paralleled the approach path. Data were collected from contiguous range locations spaced 150 m apart, which is the closest possible for the present system. Minimum range varied from approximately 2.5 to 6.0 km, limited by the antenna ground clutter return through antenna side lobes, while maximum range of data collection was typically 22.5 km. The azimuth was fixed for each approach direction, in order to minimize ground clutter interference.

The aircraft was vectored along a 3 deg glide path to the runway, using the PAR system. With this system, we could maintain the aircraft along the path, with a theoretical accuracy of 8 m in the horizontal and 2 m in the vertical, utilizing voice commands from the Air Force PAR controller, who could monitor the aircraft with a computer tracking display.

Two types of aircraft and Doppler wind comparisons were attempted. The first type we call Lagrangian, because it was an attempt to verify most accurately the Doppler winds while an aircraft was moving along the beam. In other words, we continuously collected Doppler radial velocity data along the 3 deg path while the airplane was moving through

6
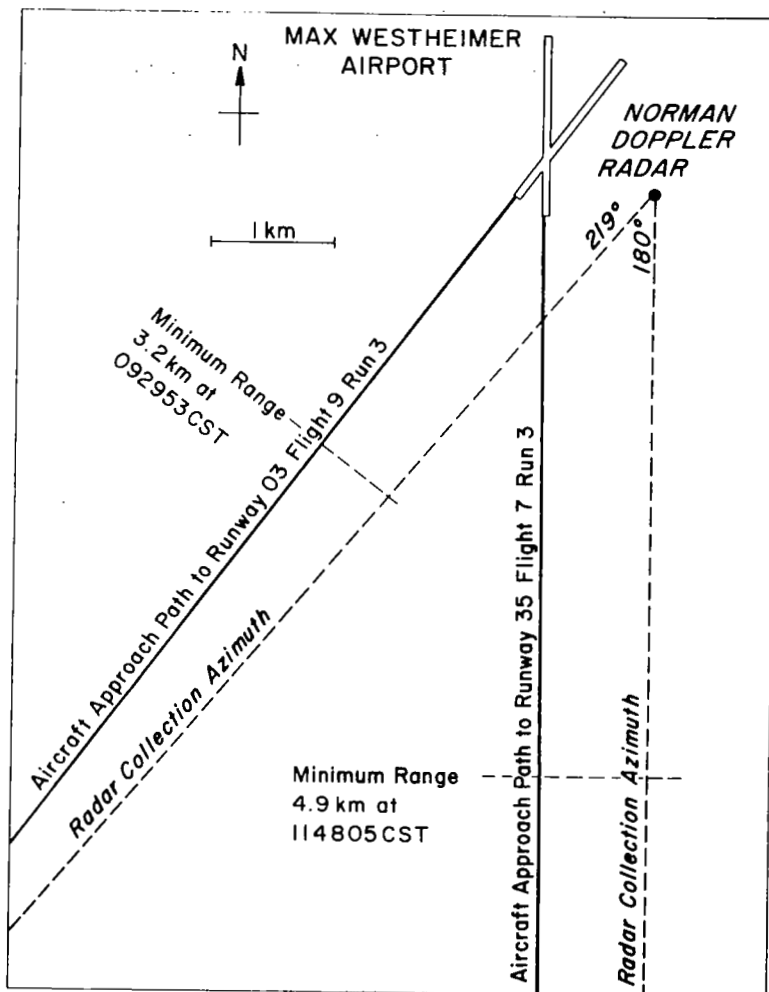
Figure 1. A map showing the runways, approach path, location, and azimuth scans for comparison experiment.

the range locations where data were collected. For the actual Lagrangian comparison, the Doppler radial velocity was computed in the first range gate immediately ahead of the airplane, which could easily be seen to progress through the Doppler data. This set of Doppler data, collected in a progressive space-time framework, was then compared point-by-point with the airplane longitudinal wind data.

A second measurement we termed Eulerian, because it was sampled instantaneously, or time-fixed, along the flight path. One sample was collected immediately prior to the start of an approach, while a second sample was collected immediately after an approach was terminated.

These two types of Doppler sampling were designed to accomplish two things. First, the Lagrangian sample provided our best "ground truth" verification of the Doppler's wind measuring accuracy when compared to aircraft-measured winds. Secondly, we wanted to know whether the Eulerian samples taken before (or after) an approach accurately represented the Lagrangian sample. In other words, is the wind shear signal coherent over the approximately 4 min. of the approach period? In a real-time test of the detection and warning system, only the Eulerian sample could provide significant advance warning.

Simultaneously, with all PAR directed Doppler wind measurements, aircraft data were collected. Both surface-based and airborne wind data were compared; the results of these comparisons are given in Chapter III.

Doppler derived winds along the approach path, for both Lagrangian and Eulerian modes, were fed into the Blick model, to obtain performance predictions. The results of these simulations are given in Chapter IV.

During the entire experiment, 43 PAR approachs were conducted. However, a post-experiment examination of the data indicated complete

8

data availability on 16 approaches. A total of 12 Queen Air and 4 Sabreliner approaches were analyzed fully. Table 1 summarizes certain details of each of these approaches.

TABLE 1

SUMMARY OF PAR CASES UNDER ANALYSIS

Date	Aircraft No.	Flight No.	Run No.	Time (CST) Start	Stop	Computer Identification Code
5- 7-79	S	6	1	115247	115447	SF6R1M07
5-14-79	S	8	1	093713	094032	SF8R1M14
5-14-79	S	8	2	095447	095822	SF8R2M14
5-14-79	S	8	3	101651	102101	SF8R3M14
4-25-79	Q	5	1	100532	100739	QF5R1A25
4-25-79	Q	5	3	104134	104342	QF5R3A25
5- 7-79	Q	7	3	114601	114805	QF7R3M07
5-14-79	Q	8	1	092537	092948	QF8R1M14
5-14-79	Q	8	2	094725	095140	QF8R2M14
5-14-79	Q	8	3	100824	101219	QF8R3M14
5-16-79	Q	9	1	084602	084811	QF9R1M16
5-16-79	Q	9	2	090649	090931	QF9R2M16
5-16-79	Q	9	3	092617	092953	QF9R3M16
6- 1-79	Q	16	1	085224	085634	QF16R1J1
6- 1-79	Q	16	2	091411	091856	QF16R2J1
6- 4-79	Q	17	2	160009	160257	QF17R2J4

S = NCAR Sabreliner
Q = NCAR Queen Air

CHAPTER III

MEASUREMENT OF WINDS ALONG THE APPROACH PATH

1. Doppler Radar Winds

Estimates of the clear-air velocity were obtained interactively from the mini-computer system at NSSL. The velocity spectrum, which consisted of the average of ten discrete velocity spectra, was displayed for each of 64 resolution volumes. Each mean velocity spectrum is displayed by 64 points or indices spanning an index value from -32 to +31. After making a rough visual estimation of the mean Doppler or expected value of the clear-air Doppler velocity, an objective estimate of the mean index, E(i), is made using

$$E(i) = \sum_{i=-\frac{M}{2}}^{\frac{M}{2}-1} iP_i \qquad (1)$$

where M is the number of indices (64), i is the index, and P_i is the power density of the spectrum at index i. In the algorithm used, spectral noise created by ground clutter is removed by limiting the range spanned by the index i to just that required to bracket the clear-air velocity spectrum. This is equivalent to reducing the spectral density outside of the clear-air velocity spectrum to zero.

Radial velocity is obtained from (1) by the relation

$$V_r = \left[\frac{-\lambda E(i)}{2MT_s}\right] \qquad (2)$$

where V is the radial velocity in m s^{-1} (defined as positive away from the radar and negative towards the radar), λ is the wavelength of the

radar in meters, i is the index of the mean Doppler, M is the total number of indices, and T is the pulse repetition time (PRT) in seconds. Velocity values obtained by the algorithm used at NSSL are accurate to better than ± 0.25 m s^{-1}. Figure 2 is a photograph of the real-time display, illustrating a wind shear situation.

During each approach, a Lagrangian data set was collected consisting of the clear-air velocity in the "cleanest" range gate ahead of the approaching aircraft. The spectral signature of the aircraft was strikingly different from a clear-air signal, so there was no difficulty in defining a "clean" range gate just in front of the aircraft. The Lagrangian velocity data were, of course, collected as a function of time and range. In general, the spatial resolution of the Lagrangian data was inferior to that of the Eulerian data. Some time was required to gather the Doppler data and average the spectra; depending on the approach speed of the aircraft and this data acquisition time, the aircraft may have flown completely through one or even two range gates. So, whereas we have velocity data with a spatial resolution of 150 m for the Eulerian cases, we often may have velocities at only every 300 m for the Lagrangian data.

Processing of the data consisted first of filtering (smoothing), using a simple three-point filter defined by

$$f_j = (1 - s)f_j + \frac{s}{2}(f_{j+1} + f_{j-1}) \qquad (3)$$

which has a response function of

$$R(s) = 1 - 2s \sin^2 (\pi\Delta x/L) \qquad (4)$$

where s is a constant that determines the filter response, j is an index, f is the value of the data at some j, and Δx is the interval between the data points. For this study, s = ½, yielding a response of

---

[1]Private communication with R. Doviak, NSSL.

12
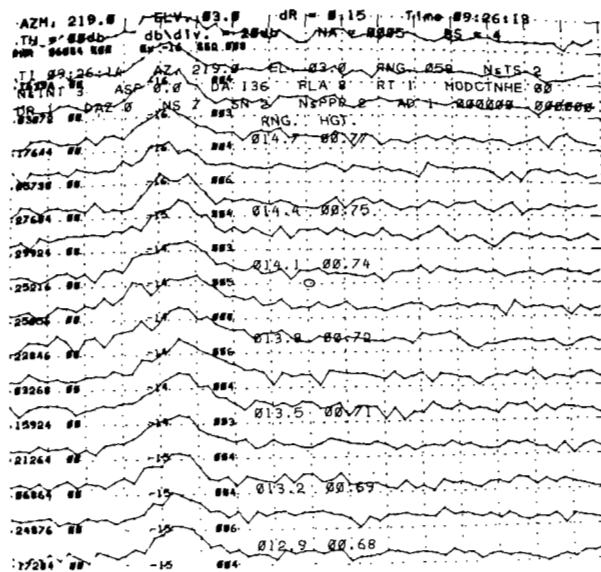
Figure 2. Photograph of the NSSL display for Queen
Air Flight 9 Run 3. Display shows 16 Doppler spectra
at each 150 m slant range, with closest range 12.9 km
(bottom) and furthest range 15.3 km (top). Clear air
velocity values range from ± 32 m s^{-1}, with typical
values for this case near 16 m s^{-1}, shown as integer
values for each spectrum.

$$R(\tfrac{1}{2}) = \cos^2 (\pi \Delta x / L) \qquad (5)$$

thus completely removing wavelengths of $2\Delta x$. This filter and its response function apply only to evenly spaced data. Unfortunately, the Lagrangian data are not necessarily evenly spaced in time or space. However, it was felt that the deviations from even spacing were not sufficient to invalidate use of this filter.

Since data spacing is on the order of 150 m for Eulerian data and 300 m for Lagrangian data, some method of interpolation must be used for plotting purposes. Further, our numerical model used requires that wind data be supplied every second, which necessitates interpolation. The most suitable interpolation scheme for these purposes was a natural cubic spline, which has several attractive features:

1) the spline passes through every data point;

2) the spline $[s_i(x)]$ is a cubic on each subinterval (x_i, x_{i+1});

3) the spline is continuous, i.e., $s_i(x_i) = s_{i+1}(x_i)$; and

4) the first and second derivatives are continuous and the integral

$$\int_{x(o)}^{x(n)} [s''(x)]^2 \, dx \qquad (6)$$

is a minimum, yielding the smoothest possible interpolation through the data.

Since there are an indefinite number of cubic splines, defined by boundary conditions, which will interpolate a set of points, and since nothing was known about the derivatives at the end points, a natural cubic spline was defined by setting the first and second derivatives at the end points to zero.

For plots of velocity as a function of range, interpolations were performed at 25 m intervals, and for plots of velocity as a function of

time, interpolations were performed at 0.5 sec. intervals. Eulerian data were plotted as a function of time after a space-to-time conversion using the mean speed of the aircraft down the approach, defined by

$$\frac{R_{max} - R_{min}}{\Delta t} = \overline{V} \qquad (7)$$

where R_{max} is the range of the most distant range gate used in the Lagrangian data, R_{min} is the range of the closest range gate, and t is the number of seconds taken to traverse the distance $(R_{max} - R_{min})$.

2. Aircraft Measured Winds

For each of the 16 PAR approaches studied in detail, the aircraft wind data were collected at 8 Hz, and examined at 1 Hz after a running average was applied. The primary wind variable examined was the longitudinal component (headwind, tailwind) along the flight track. Aircraft position was determined initially by an inertial navigation system (INS). Aircraft range from the Norman Doppler radar was calculated from the Doppler data, since the aircraft provided a strong radar return, and could easily be seen to move along the beam. We found that the aircraft INS position was often between 0.5 and 1.5 km different than the range position provided by the Doppler radar. Because of well-known nonlinear and uncorrectable errors in the INS, we decided to use the Doppler signal as the "correct" range for the comparisons. Unfortunately, we could not locate the aircraft position lateral to the beam. Since the radar beam and approach paths were not colocated (see Figure 1), there was an approximate 1 km average uncorrected lateral position error.

3. Comparison Between Doppler Radar, Aircraft Winds, and other Flight
   Parameters.

We have examined 12 Queen Air approaches, and 4 Sabreliner approaches.
When we compared Doppler radar and aircraft longitudinal wind data, using
a subjective judgment, 75% of the 16 approaches compared well, while 25% did
not. To illustrate this further, we chose two cases to present in detail
here.

   a. 16 May 1979 - Queen Air Flight 9 Run 3

   On this day, we made three approaches to runway 03 (north-
northeast bound) to Westheimer, during a clear-air low-level southerly
jet situation, in mid-morning. The approach began at 092617 CST and
ended at 092953, with a start range from the Doppler of 20.5 km, and
a final range of 3.7 km. The approach lasted 3 min, 36 sec. Figure 3a
presents a vertical view of the approach, with aircraft height, in
meters above Norman radar, expressed as a function of time. Figure 3b
represents the height of the aircraft, expressed as deviation in meters
from the glide slope as a function of time. Notice the phugoidal-like
oscillation in the altitude. These oscillations can be seen in the
airspeed and pitch angle data, as a function of time (Figures 3c-e).

   Figure 3f represents the Lagrangian comparison between the
aircraft longitudinal wind and the Doppler radial wind, along the
glide path, as a function of time. Several interesting points can
be seen. The resolution/smoothing difference between the aircraft
and Doppler data is evident. While the absolute comparison appears
quite good, there are obvious differences, particularly farther
out from the radar. Finally, small-scale wave-like and turbulent

16

WND SHR   QF9R3M16 QF9R3M16   926- 929
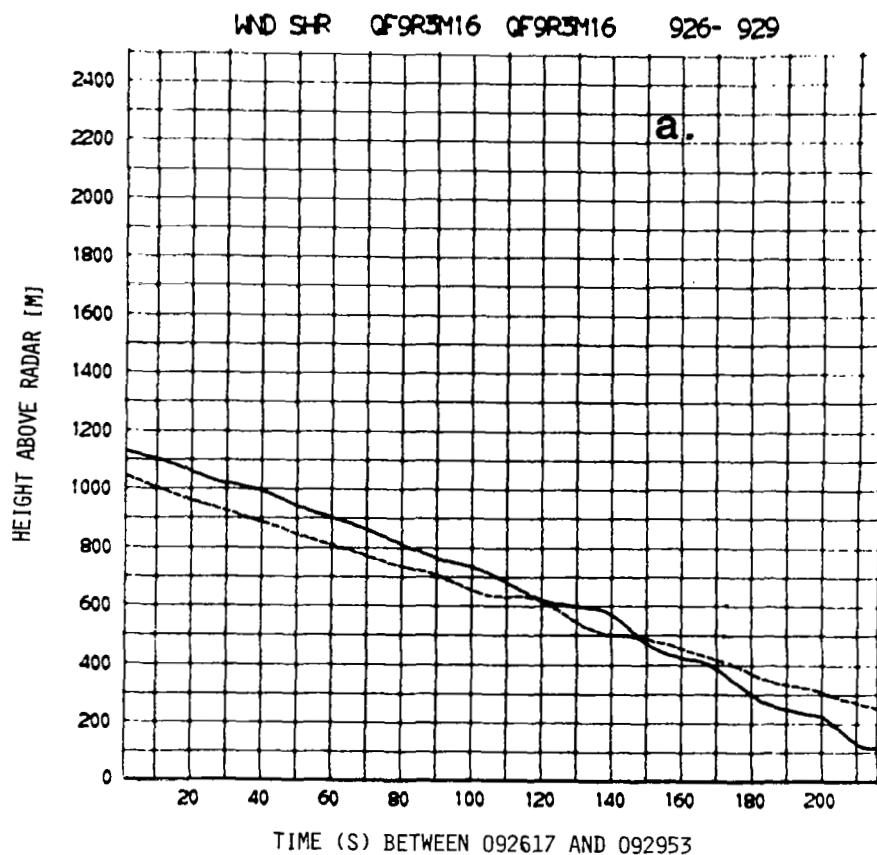
Figure 3a. First of 8 data panels for Queen Air
approach on 16 May 1979, designated as Flight 9 Run 3
(approach code QF9R3M16 on Table 1). This shows air-
craft altitude (m) above the Norman Doppler radar, as
a function of time. Solid line is actual aircraft
altitude, while dashed line represents the calculated
altitude as determined by the Blick numerical simu-
lation model, applied to the Eulerian Before case;
results of the model will be discussed in Chapter IV.

17

WND SHR   QF9R3M16 QF9R3M16   926- 929

b.

TIME (S) BETWEEN 092617 AND 092953
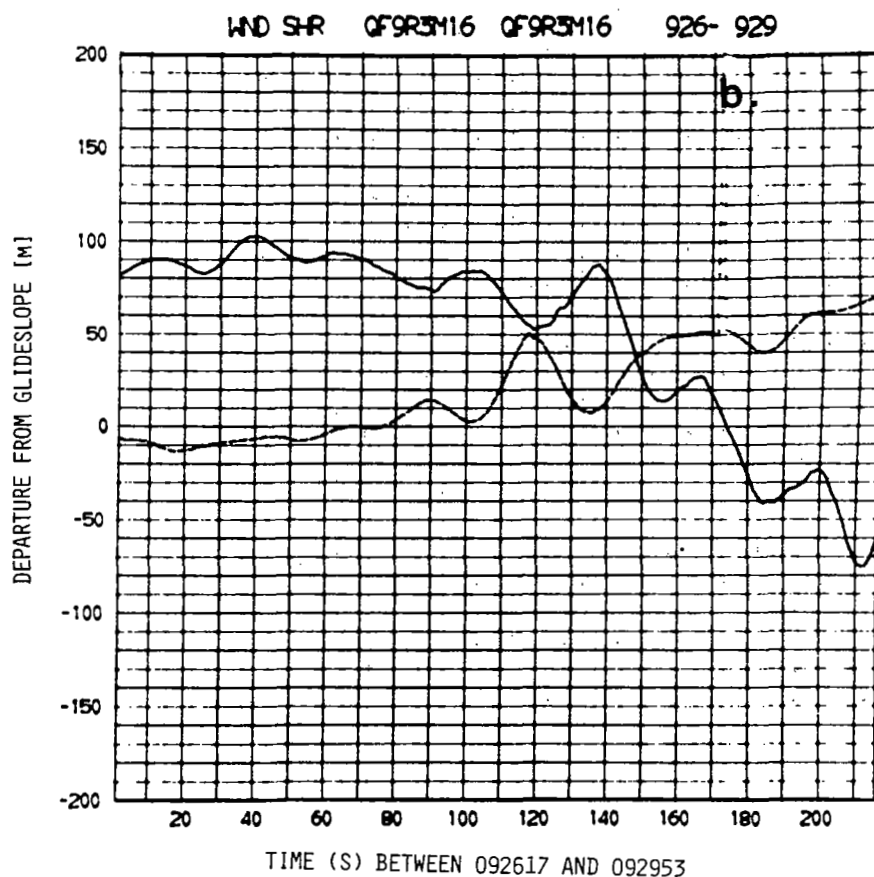
Figure 3b. QF9R3M16 showing aircraft (solid line) and
model (dashed line) altitude (m) departure from a 3 deg
glide slope path to the radar, with positive values
representing altitude departures above the path, all as
function of time. The lack of phasing here and in 3c,d,e,
is apparently due to the inaccuracy of the model to predict
precise details in weak shear conditions.
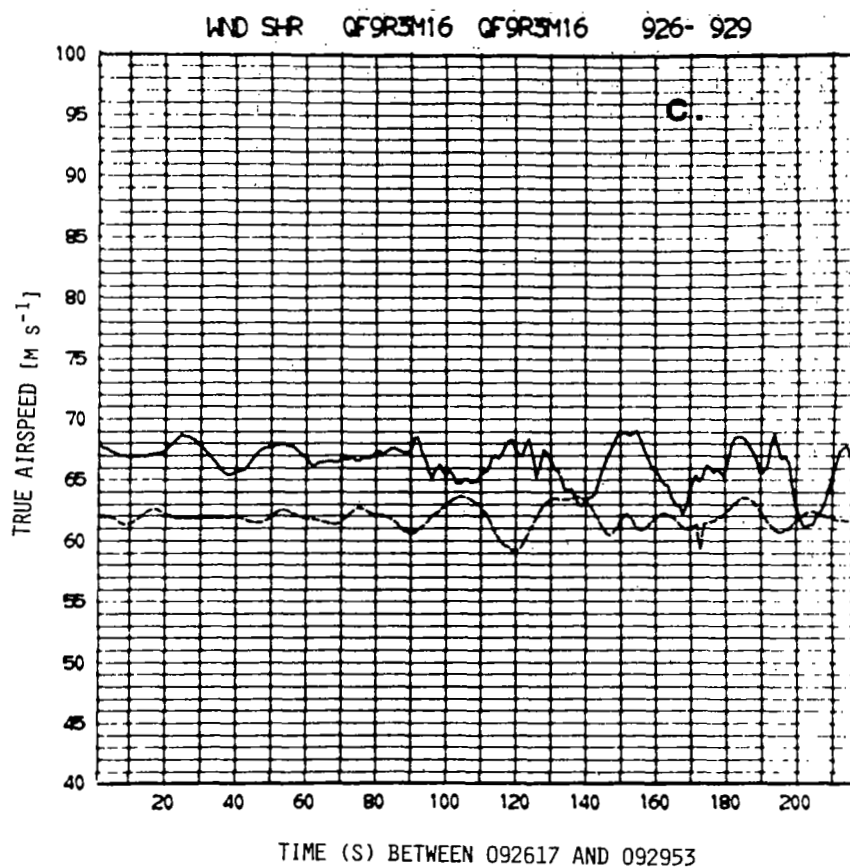
Figure 3c. QF9R3M16 showing aircraft and model true
airspeed (m s⁻¹) as a function of time.

19
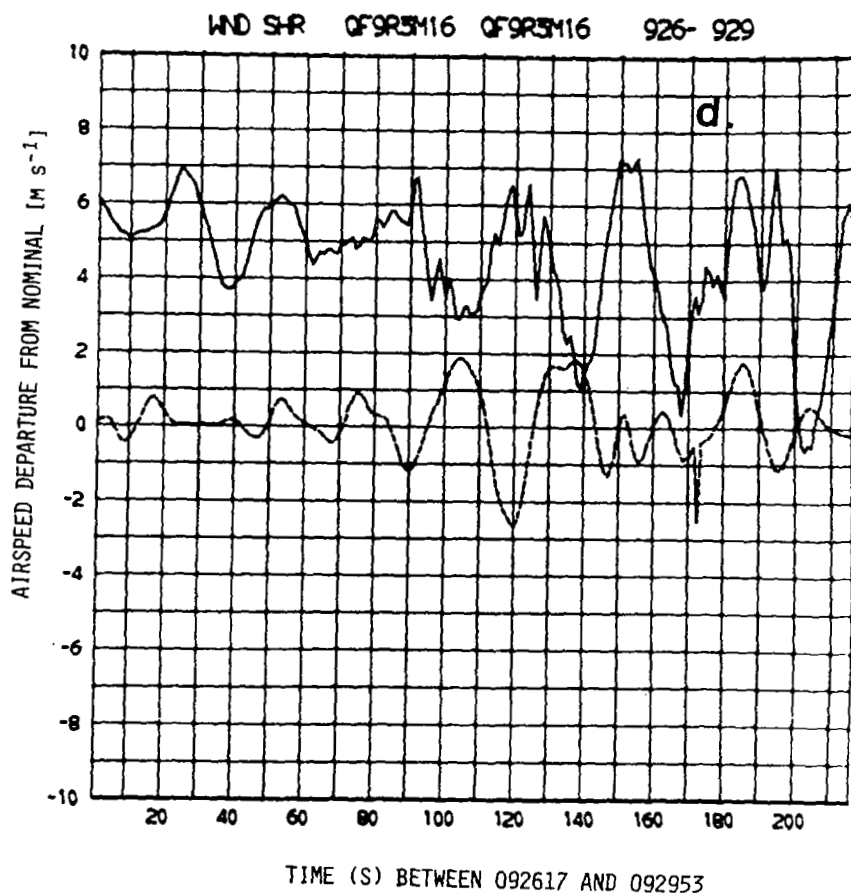
Figure 3d. QF9R3M16 showing aircraft and model air-
speed departure nominal (or no wind) approach speed
of 61.77 m s⁻¹ (120 knots); airspeeds higher than
nominal are positive.

WND SHR   QF9R3M16 QF9R3M16   926- 929

e.

PITCH ANGLE [DEG]

TIME (S) BETWEEN 092617 AND 092953
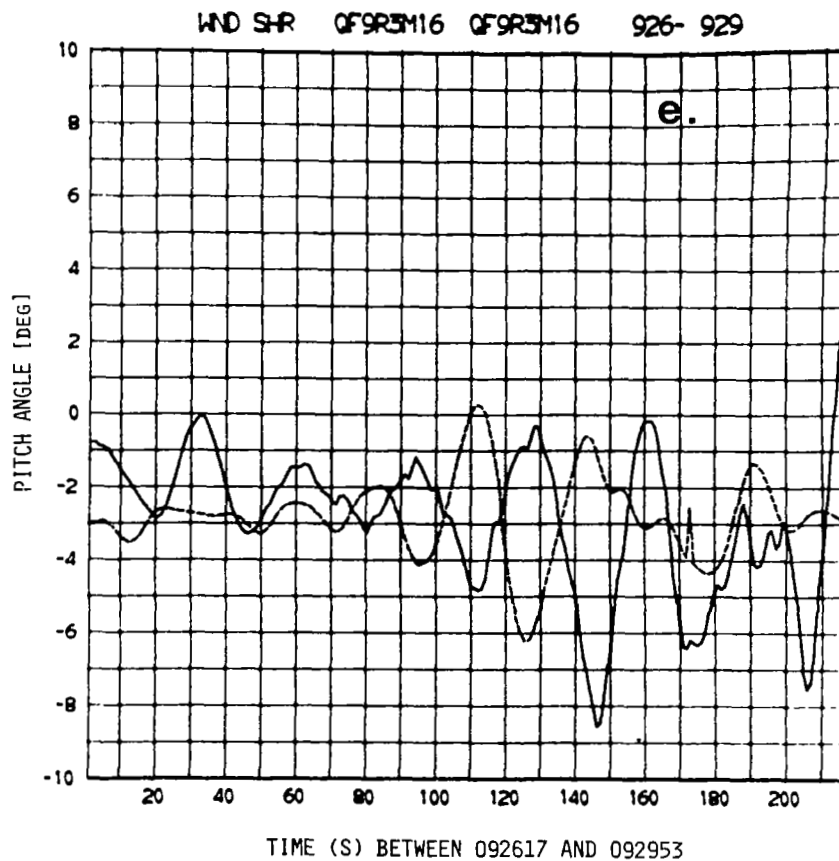
Figure 3e. QF9R3M16 showing aircraft and model pitch angle (deg) as a function of time.

WND SHR QF9R3M16 QF9R3M16 926- 929

f.

LAGRANGIAN RADIAL VELOCITY [m s^{-1}]

TIME (S) BETWEEN 092617 AND 092953
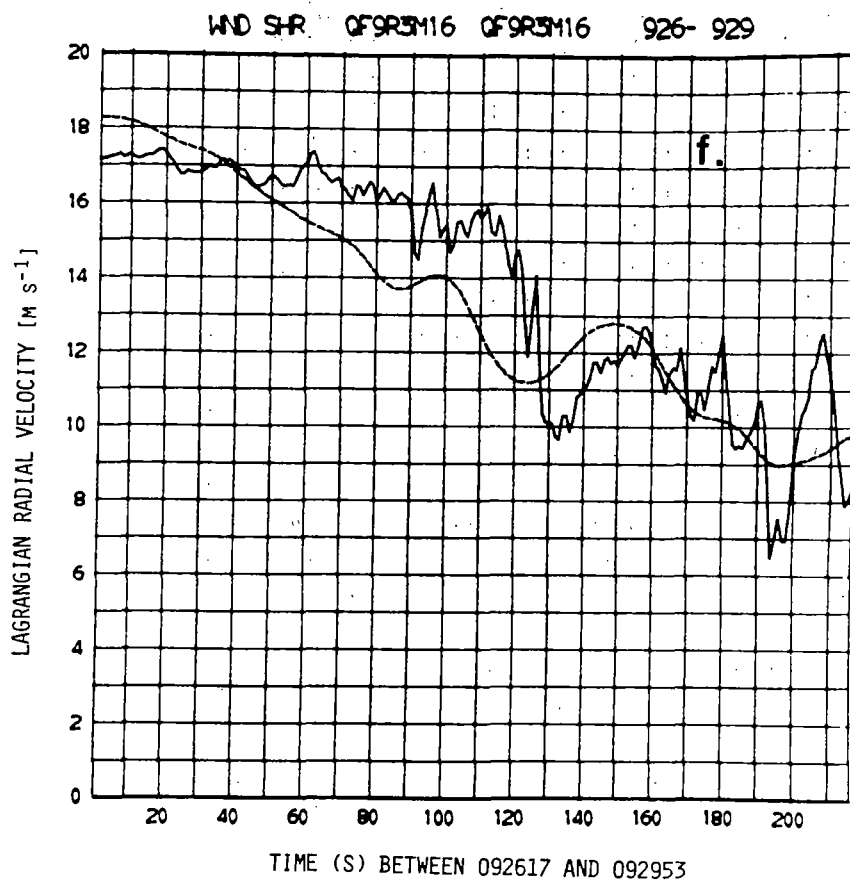
Figure 3f. QF9R3M16 comparison of aircraft (solid
line) longitudinal wind (m s^{-1}) and Lagrangian
Doppler velocity (m s^{-1}) (dashed line) as a function
of time.

22
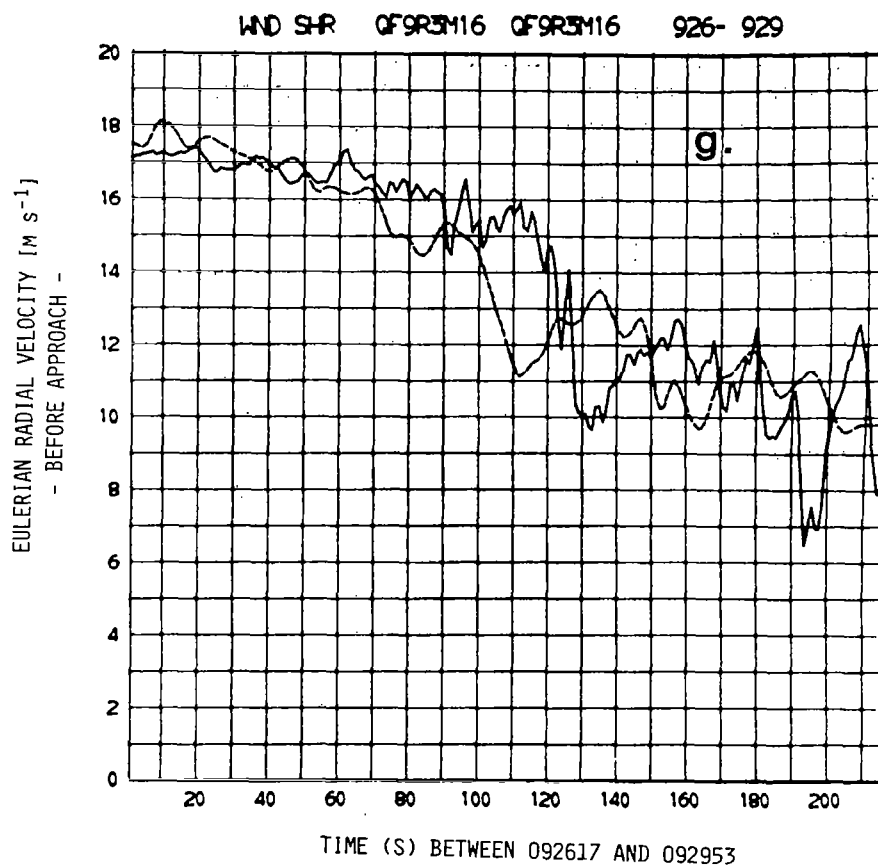
Figure 3g. QF9R3M16 comparison of aircraft (solid line) longitudinal wind and Eulerian Doppler velocity (dashed line) taken 1 s immediatley before the start of the approach.

Figure 3h. QF9R3M16 comparison for Eulerian Doppler velocity taken 1 s immediately after the end of the approach.

24
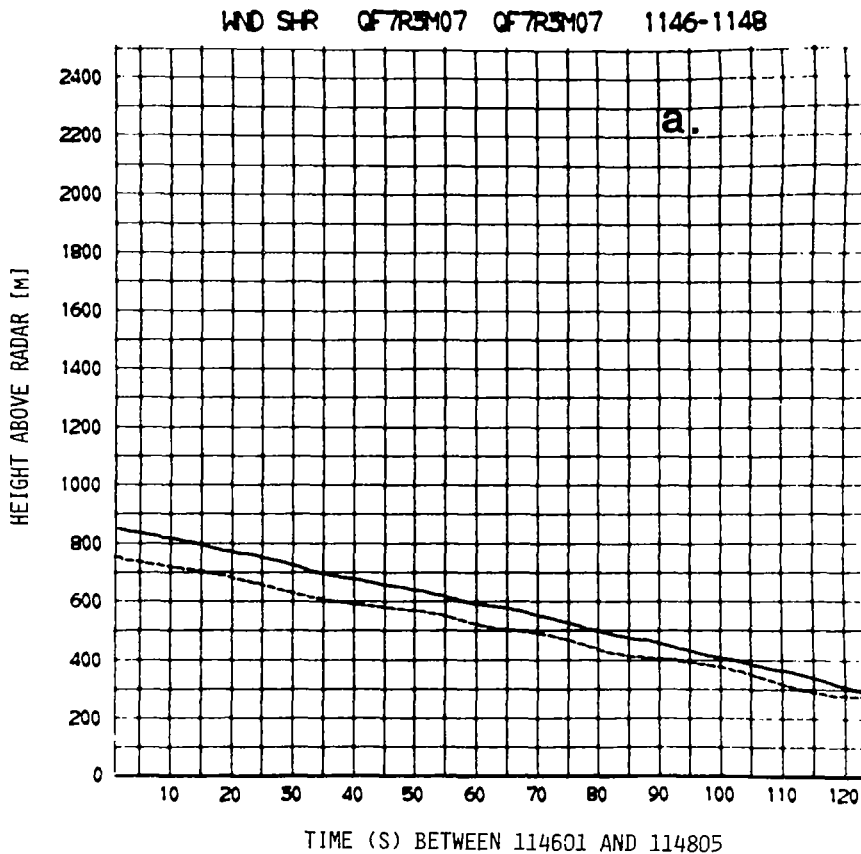
Figure 4a. First of 8 data panels for Queen Air
approach on 7 May 1979, designated as Flight 7
Run 3 (approach code QF7R3M07 on Table 1). This
shows aircraft altitude (m) above the Norman Doppler
radar, as a function of time. Solid line is actual
aircraft altitude, while dashed line represents the
calculated altitude as determined by the Blick
numerical simulation model, applied to the Eulerian
Before case; results of the model will be discussed
in Chapter IV.

25

Figure 4b. QF7R3M07 showing aircraft (solid line)
and model (dashed line) altitude (m) departure from
a 3 deg glide slope path to the radar, with positive
values representing altitude departures above the
path, all as function of time.

WND SHR   QF7R3M07 QF7R3M07   1146-1148

TIME (S) BETWEEN 114601 AND 114805
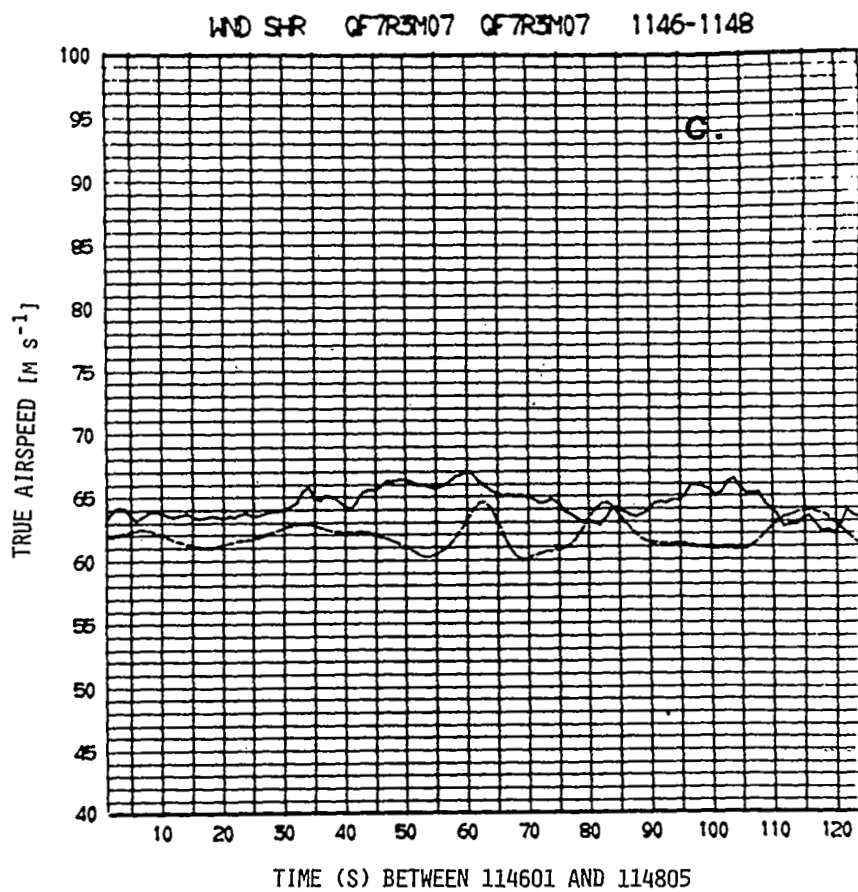
Figure 4c. QF7R3M07 showing aircraft and model true airspeed (m s^{-1}) as a function of time.

27
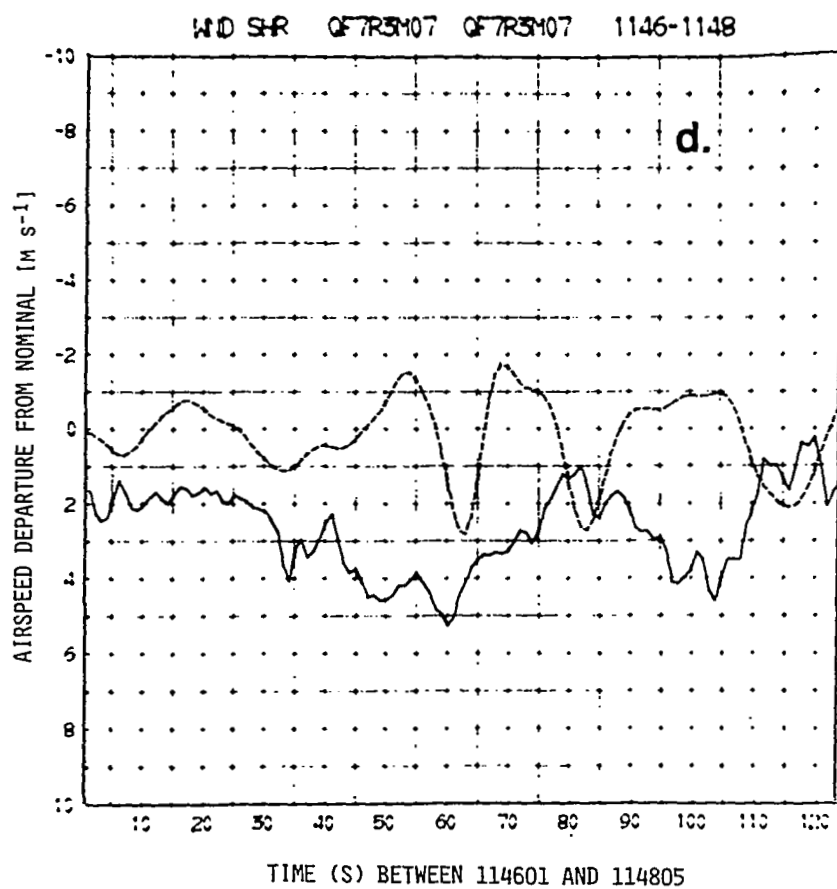
Figure 4d. QF7R3M07 showing aircraft and model airspeed departure nominal (or no wind) approach speed of 61.77 m s^{-1} (120 knots); airspeeds higher than nominal are positive.

WND SHR   QF7R3M07 QF7R3M07   1146-1148
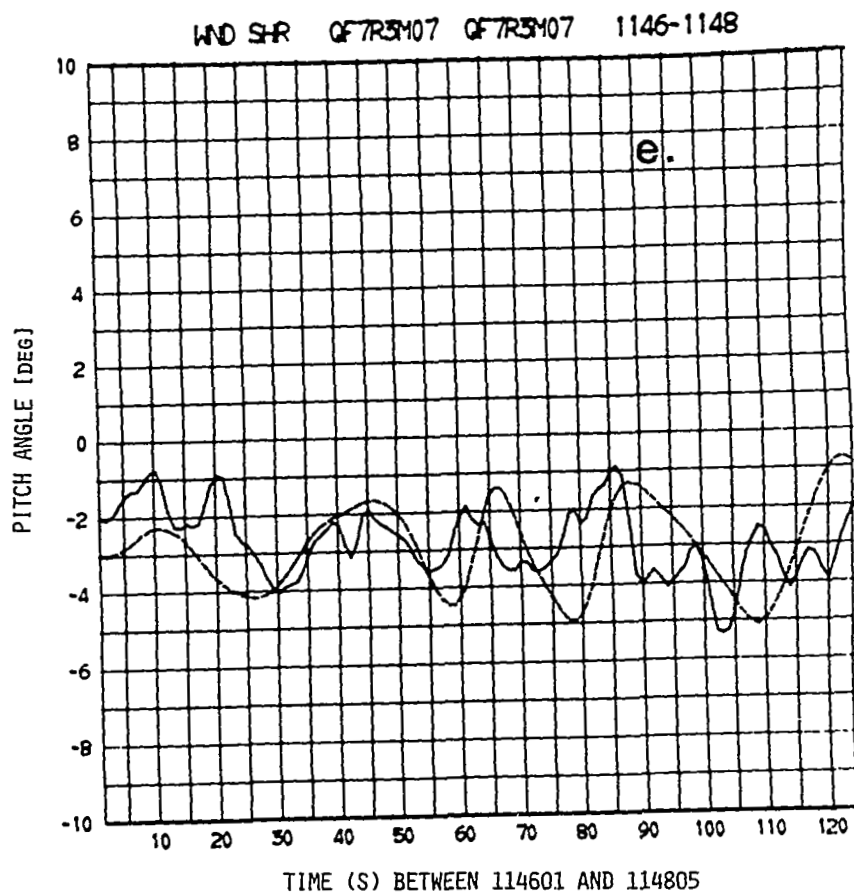
Figure 4e. QF7R3M07 showing aircraft and model pitch
angle (deg) as a function of time.
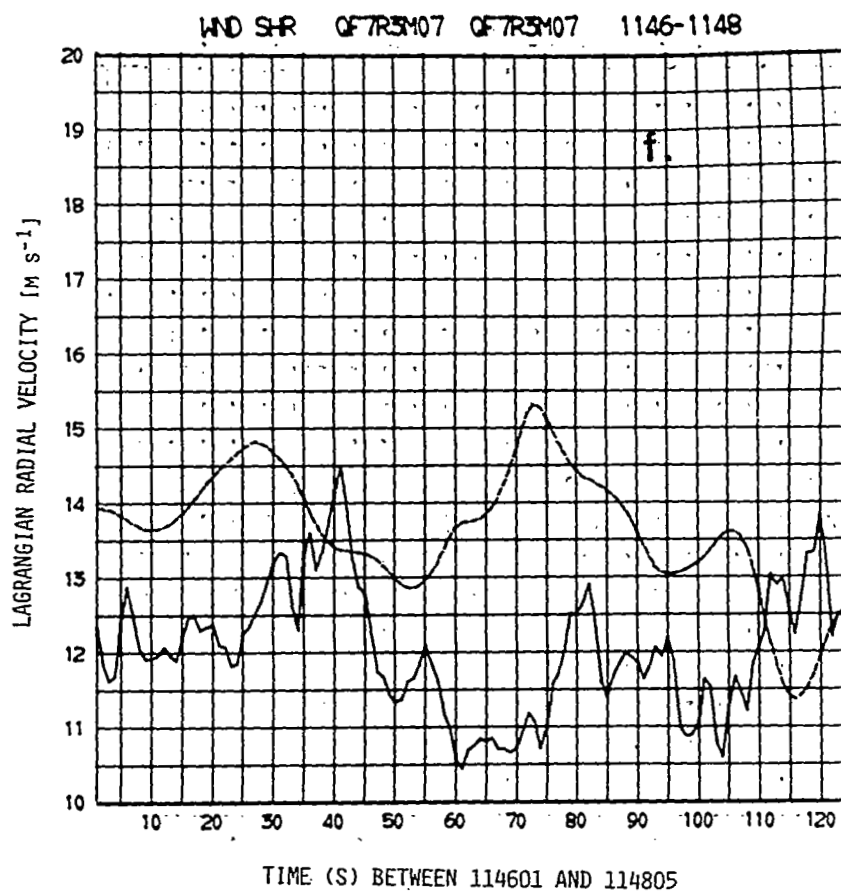
Fugure 4f.   QF7R3M07 comparison of aircraft (solid line) longitudinal wind (m s^{-1}) and Lagrangian Doppler velocity (m s^{-1}) (dashed line) as a function of time.

WND SHR   QF7R3M07 QF7R3M07   1146-1148

g.

EULERIAN RADIAL VELOCITY [M s⁻¹]
- BEFORE APPROACH -

TIME (S) BETWEEN 114601 AND 114805

Figure 4g. QF7R3M07 comparison of aircraft (solid
line) longitudinal wind and Eulerian Doppler
velocity (dashed line) taken 1 s immediately before
the start of the approach.

WND SHR   QF7R3M07   QF7R3M07   1146-1148

EULERIAN RADIAL VELOCITY [M s⁻¹] - AFTER APPROACH -

TIME (S) BETWEEN 114601 AND 114805
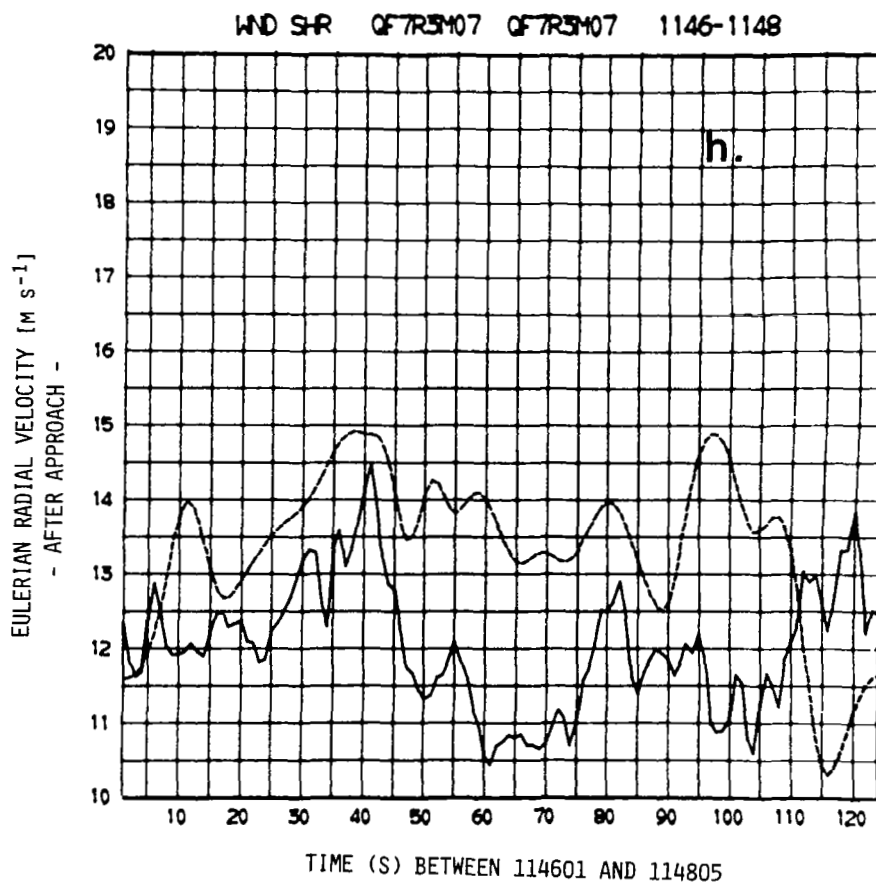
Figure 4h. QF7R3M07 comparison for Eulerian Doppler velocity taken 1 s immediately after the end of the approach.

disturbances are evident in the higher-resolution aircraft data. Remember, this comparison represents the best comparison, where the aircraft and Doppler data were collected in as close a space-time framework as possible. Of course, to make this comparison possible, the aircraft had to make the approach, a situation unsuitable for our real-time detection and warning system. In that system, we want to be able to monitor the wind shear continuously, to anticipate adverse conditions along the path, prior to an airplane actually beginning an approach.

Figures 3g and 3h represent Eulerian velocity comparisons, with the Doppler data collected 1 sec. immediately prior to the start of the approach, and 1 sec. immediately following the termination of the approach, respectively. Two obvious features are apparent. The general nature of the comparison does not change. The Eulerian profiles are not significantly different from the Lagrangian profile. However, the position of the smaller-scale features do shift somewhat, suggesting that waves or turbulent eddies are moving through the data.

b. _7 May 1979 - Queen Air Flight 7 Run 3_

We would be unfair if we failed to describe one of the poor cases. The wind shear situation is considerably less dramatic than the previous one. The approach began at 114601 at a range of 14.4 km, and ended at 114805 at a minimum range of 5 km, taking 2 min 4 sec to complete. The approach was made to runway 35 (north-bound) at Westheimer field.

Figures 4 a-h give results presented identically to Figures 3a - h. No obvious wind shear is evident along the flight path,

such as a penetration through a low-level jet, as in the previous example.

However, certain wave-like fluctuations (2 to 3 m s^{-1} variation) are

evident. Furthermore, no clear phugoidal oscillation is present in air-

craft, altitude, airspeed, and pitch angle data. Unfortunately, the most

obvious impression is the lack of general or absolute agreement between air-

craft and Doppler wind data. However, when we look at the smaller-scale

fluctuations, we see a similarity in scale, although seemingly out of phase.

This impression becomes slightly clearer when we compare the Lagrangian

case (Figure 4f) to the two Eulerian cases (Figures 4g-h). Our only

explanation for the lack of phasing pertains to the model's apparent inability

to predict weak wind shear situations accurately; we will discuss this later

in more detail.

In Figures 5-18, we present the remainder of the comparisons. We

give only the altitude variations from the glide slope, similar to panel b

in Figures 3 and 4, and the comparison between the Lagrangian Doppler and

aircraft winds, similar to panel f for Figures 3 and 4. Note that the

altitude deviation was unavailable for the last case QF17R2J4, or Figure 18.

The most obvious feature of these comparisons has been the remarkably

good agreement between the aircraft and Doppler data. This is particularly

true for case (a) and for approximately 75% of the cases examined. Further-

more, we were pleased with the apparent coherence or representativeness of

the Eulerian profiles over the 3 to 4 min of the approach periods, indicating

that such a data sample, when processed to provide a quantitative estimate

of approach deterioration, likely would be suitable. One important caution

should be considered: the comparisons given here are for essentially non-

thunderstorm related shears, so a good 3 to 4 min coherence might be

expected. In the case of the microburst phenomenon discussed by Fujita

Figure 5a. SF6R1M07 showing aircraft (solid line) and model (dashed line) altitude (m) departure from a 3 deg glide slope path to the radar, with positive values representing altitude departures above the path, all as function of time.
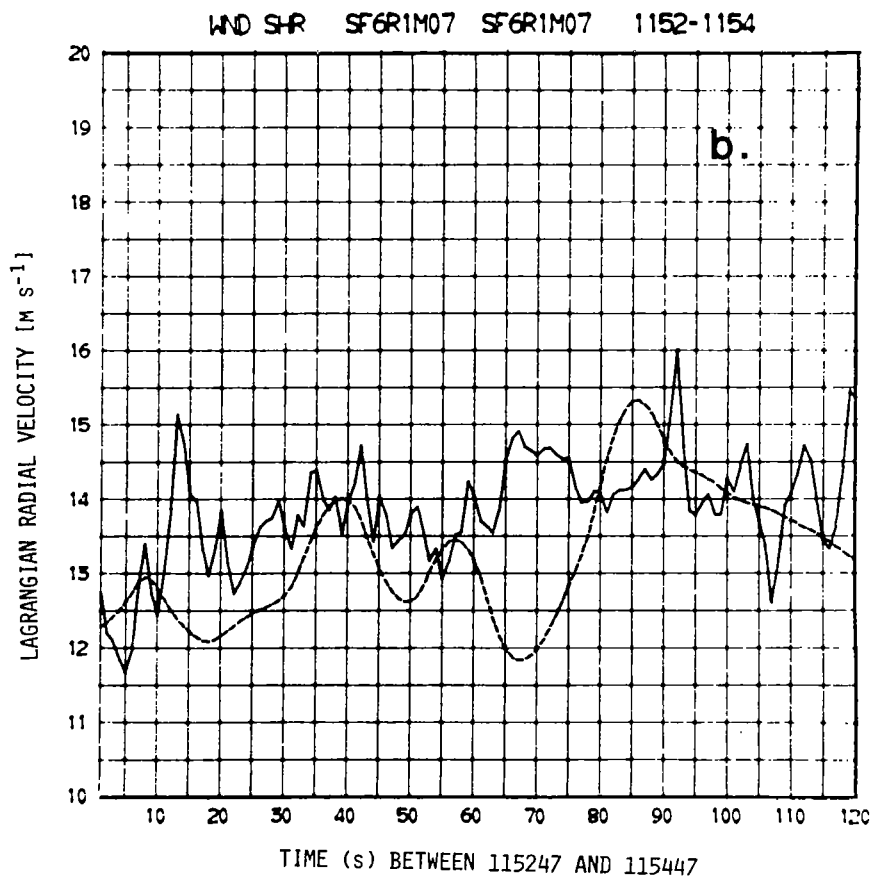
Figure 5b. SF6R1M07 comparison of aircraft (solid line) longitudinal wind (m s^{-1}) and Lagrangian Doppler velocity (m s^{-1}) (dashed line) as a function of time.
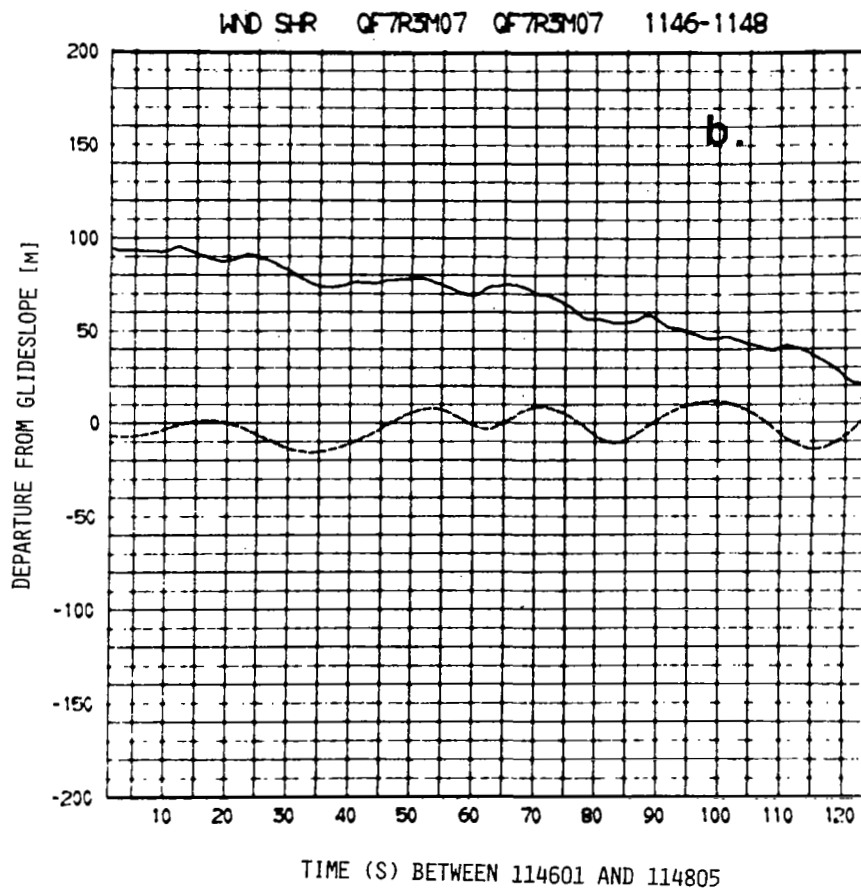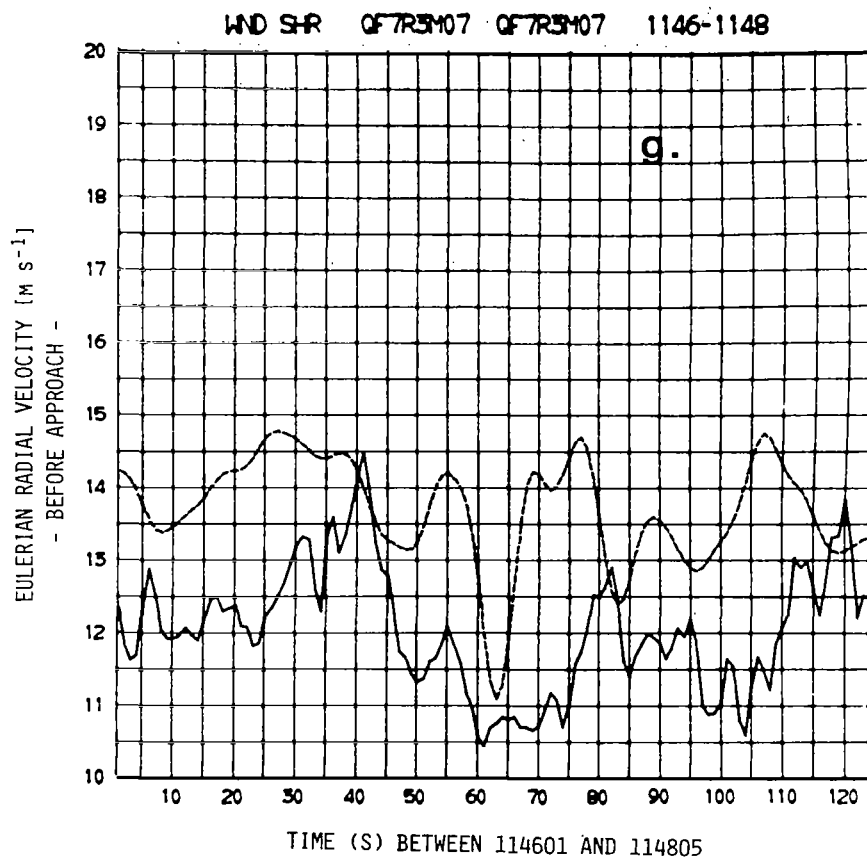
WND SHR   SF8R1M14 SF8R1M14   957- 940

Figure 6a. SF8R1M14 showing aircraft (solid line)
and model (dashed line) altitude (m) departure from
a 3 deg glide slope path to the radar, with positive
values representing altitude departures above the
path, all as function of time.

37
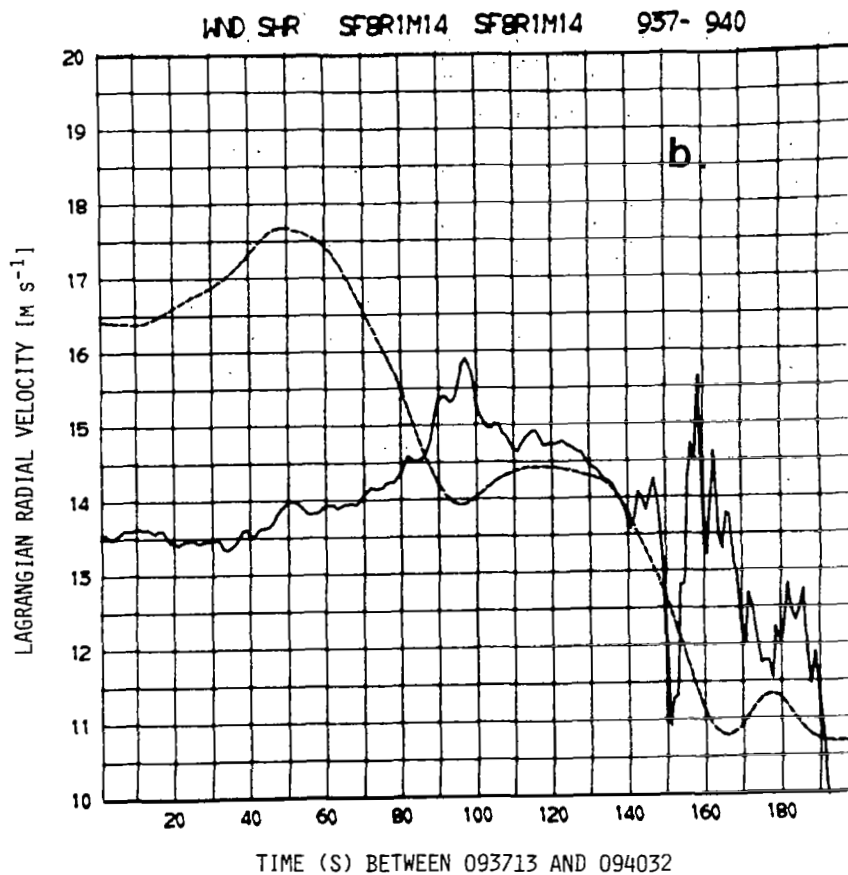
Figure 6b. SF8R1M14 comparison of aircraft (solid
line) longitudinal wind (m s⁻¹) and Lagrangian
Doppler velocity (m s⁻¹) (dashed line) as a function
of time.

Figure 7a. SF8R2M14 showing aircraft (solid line) and
model (dashed line) altitude (m) departure from a 3 deg
glide slope path to the radar, with positive values
representing altitude departures above the path, all as
function of time.

Figure 7b. SF8R2M14 comparison of aircraft (solid line) longitudinal wind (m s⁻¹) and Lagrangian Doppler velocity (m s⁻¹) (dashed line) as a function of time.

WND SHR   SF8R3M14   SF8R3M14   1016-1021
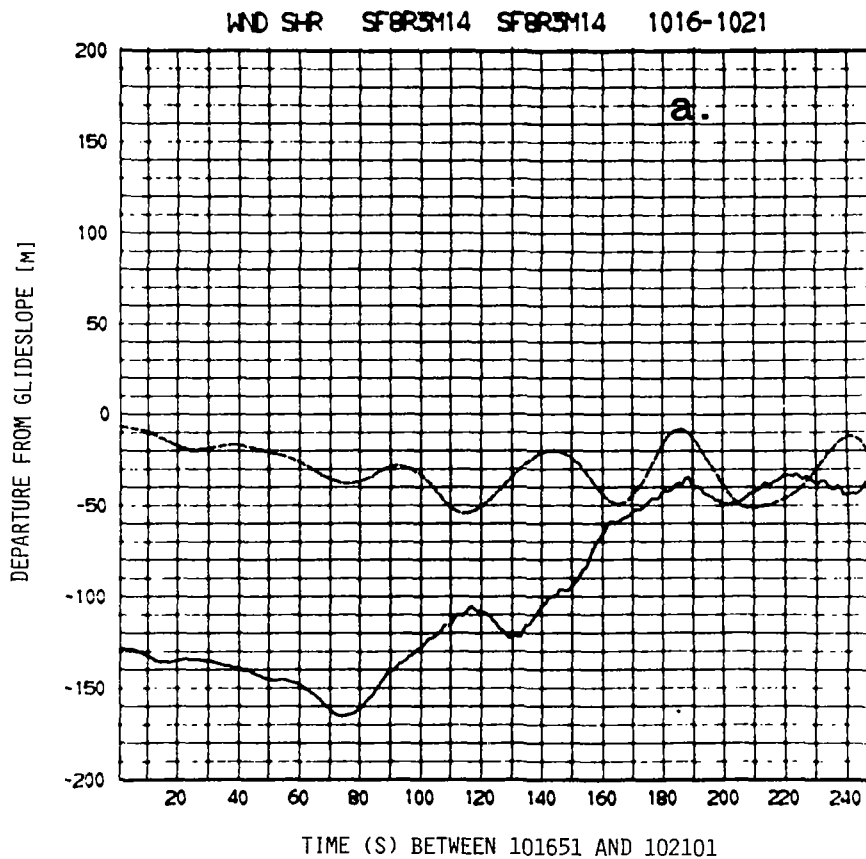
Figure 8a. SF8R3M14 showing aircraft (solid line)
and model (dashed line) altitude (m) departure from
a 3 deg glide slope path to the radar, with positive
values representing altitude departures above the
path, all as function of time.

41
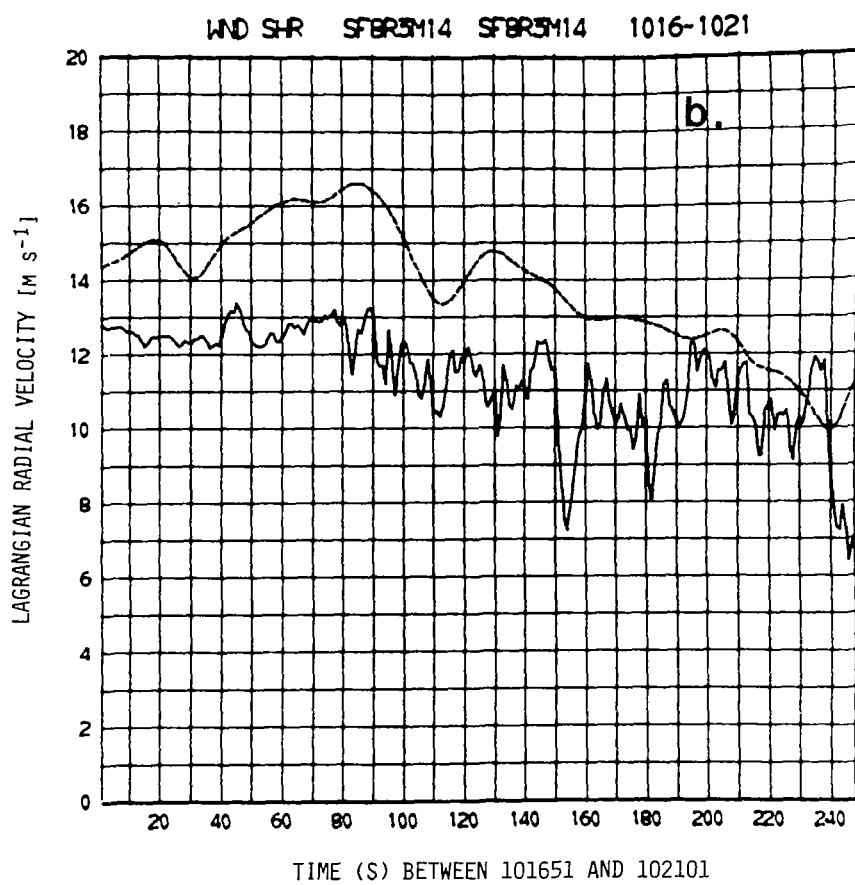
Figure 8b. SF8R3M14 comparison of aircraft (solid line) longitudinal wind (m s^{-1}) and Lagrangian Doppler velocity (m s^{-1}) (dashed line) as a function of time.
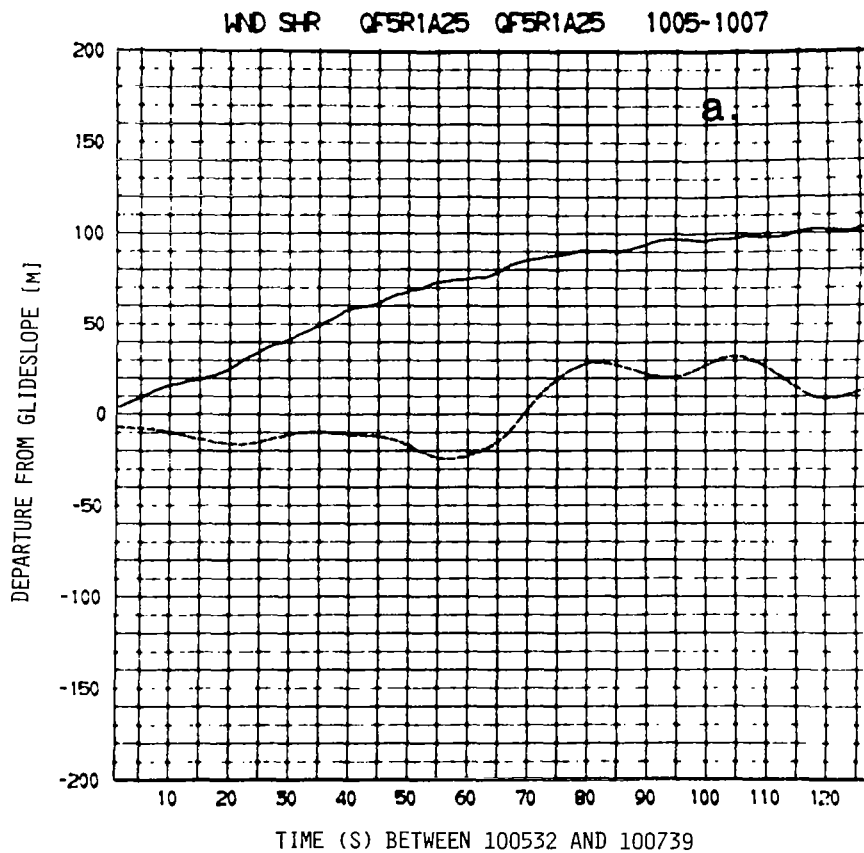
Figure 9a. QF5R1A25 showing aircraft (solid line) and model (dashed line) altitude (m) departure from a 3 deg glide slope path to the radar, with positive values representing altitude departures above the path, all as function of time.

43

WND SHR   QF5R1A25   QF5R1A25   1005-1007

b.

LAGRANGIAN RADIAL VELOCITY [m s⁻¹]

TIME (S) BETWEEN 100532 AND 100739

Figure 9b. QF5R1A25 comparison of aircraft (solid line) longitudinal wind (m s^{-1}) and Lagrangian Doppler velocity (m s^{-1}) (dashed line) as a function of time.

WND SHR   QF8R1M14   QF8R1M14   925- 929
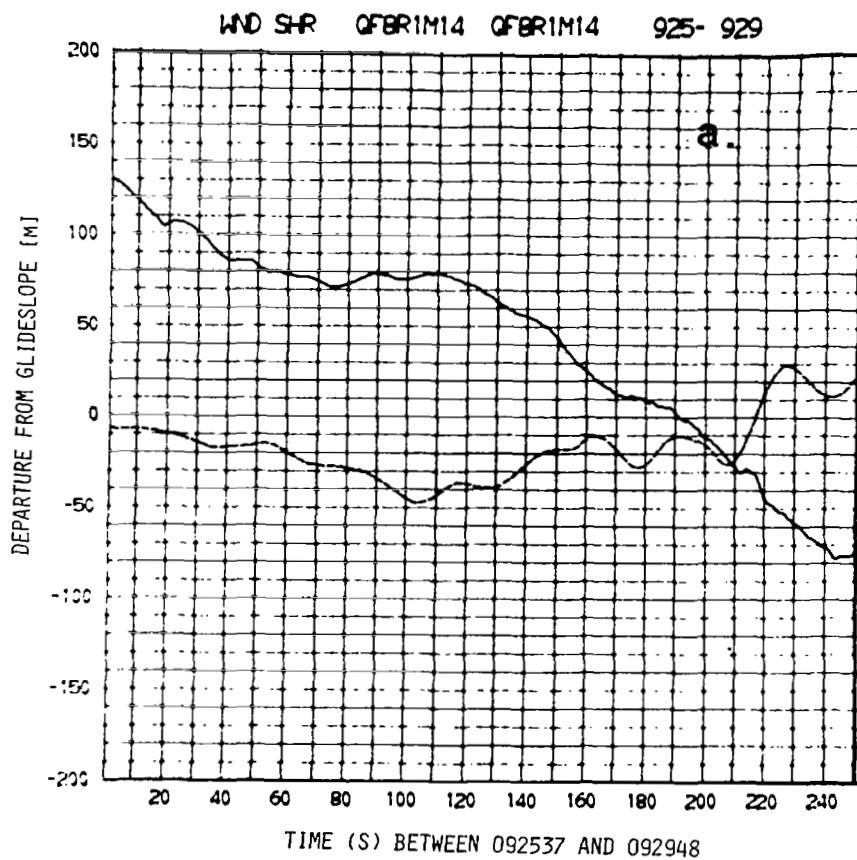
Figure 11a. QF8R1M14 showing aircraft (solid line) and model (dashed line) altitude (m) departure from a 3 deg glide slope path to the radar, with positive values representing altitude departures above the path, all as function of time.

47

WND SHR   QF8R1M14 QF8R1M14   925- 929

LAGRANGIAN RADIAL VELOCITY [M s⁻¹]

b.

TIME (S) BETWEEN 092537 AND 092948

Figure 11b. QF8R1M14 comparison of aircraft (solid line) longitudinal wind (m s⁻¹) and Lagrangian Doppler velocity (m s⁻¹) (dashed line) as a function of time.
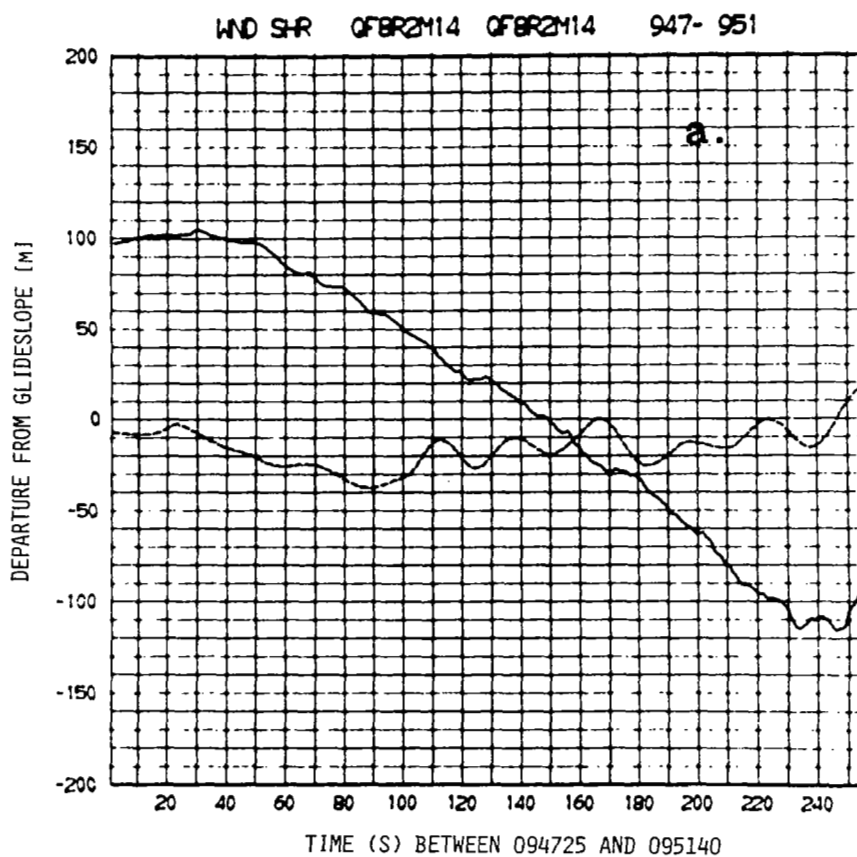
Figure 12a. QF8R2M14 showing aircraft (solid line) and model (dashed line) altitude (m) departure from a 3 deg glide slope path to the radar, with positive values representing altitude departures above the path, all as function of time.

WND SHR   QF8R2M14   QF8R2M14   947- 951
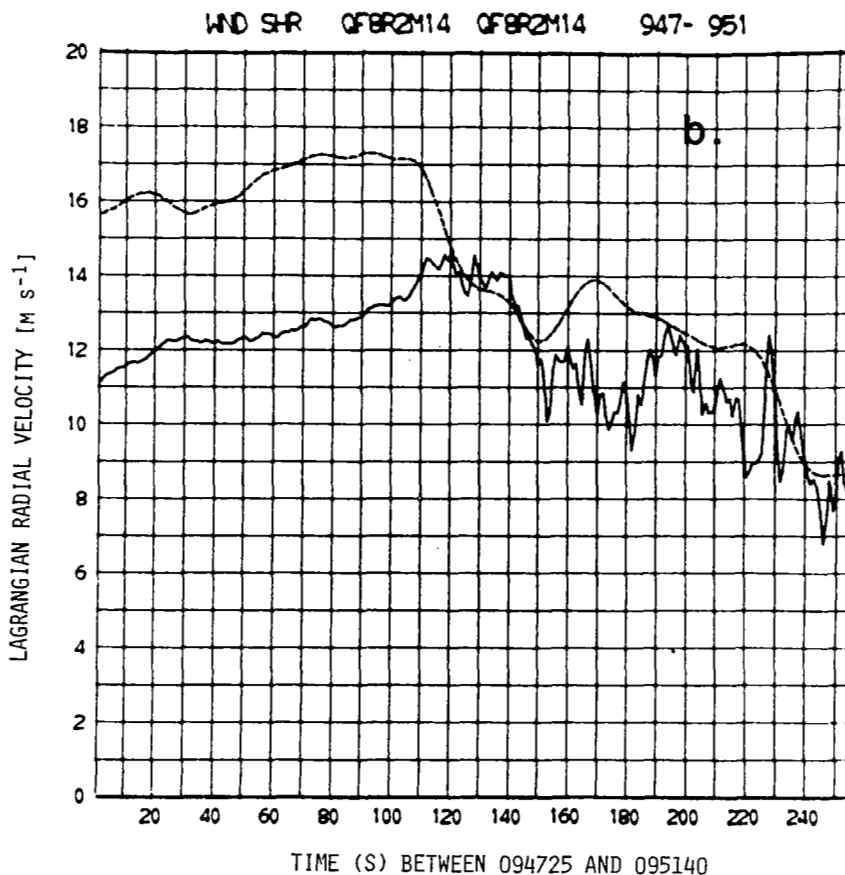
Figure 12b. QF8R2M14 comparison of aircraft (solid line) longitudinal wind (m s^{-1}) and Lagrangian Doppler velocity (m s^{-1}) (dashed line) as a function of time.

50
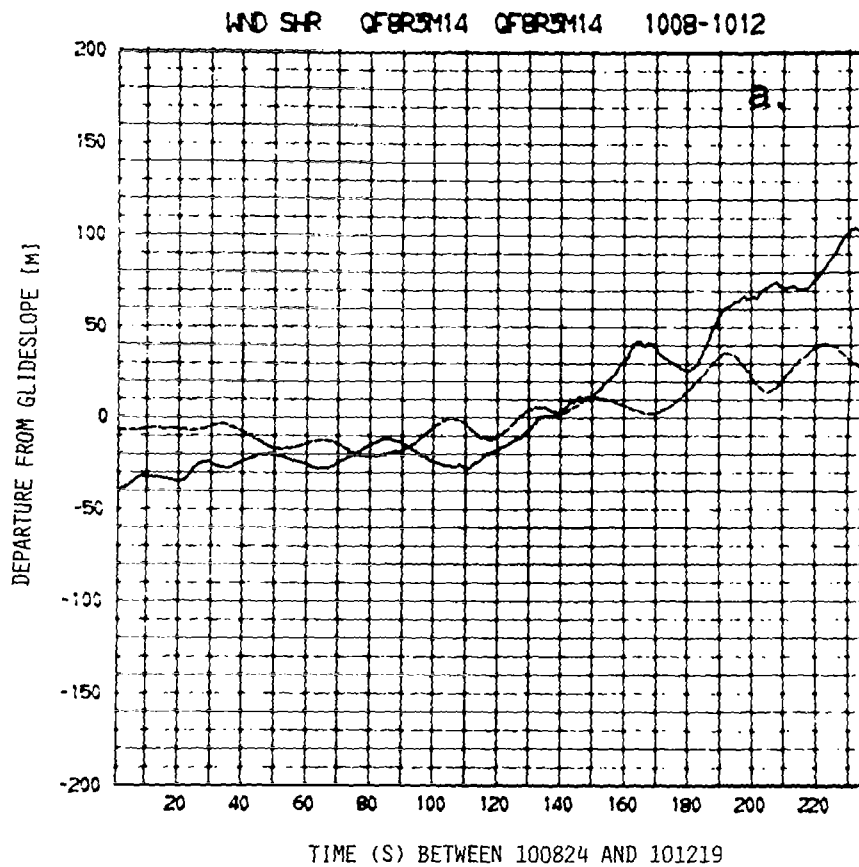
Figure 13a. QF8R3M14 showing aircraft (solid line) and model (dashed line) altitude (m) departure from a 3 deg glide slope path to the radar, with positive values representing altitude departures above the path, all as function of time.
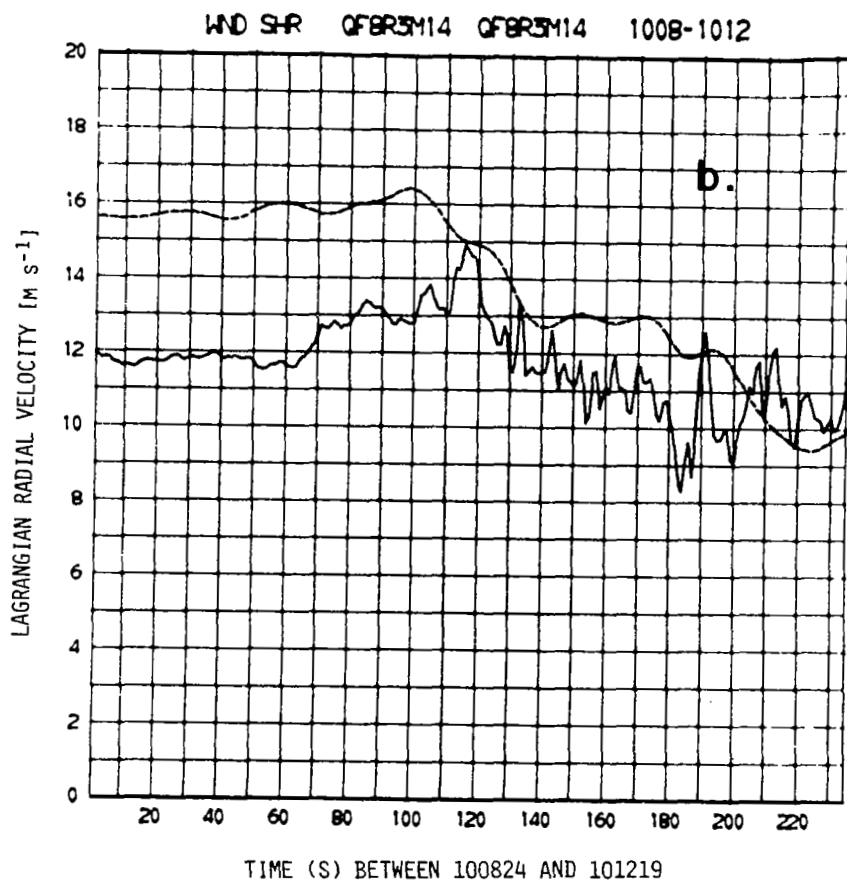
Figure 13b. QF8R3M14 comparison of aircraft (solid line) longitudinal wind (m s^{-1}) and Lagrangian Doppler velocity (m s^{-1}) (dashed line) as a function of time.
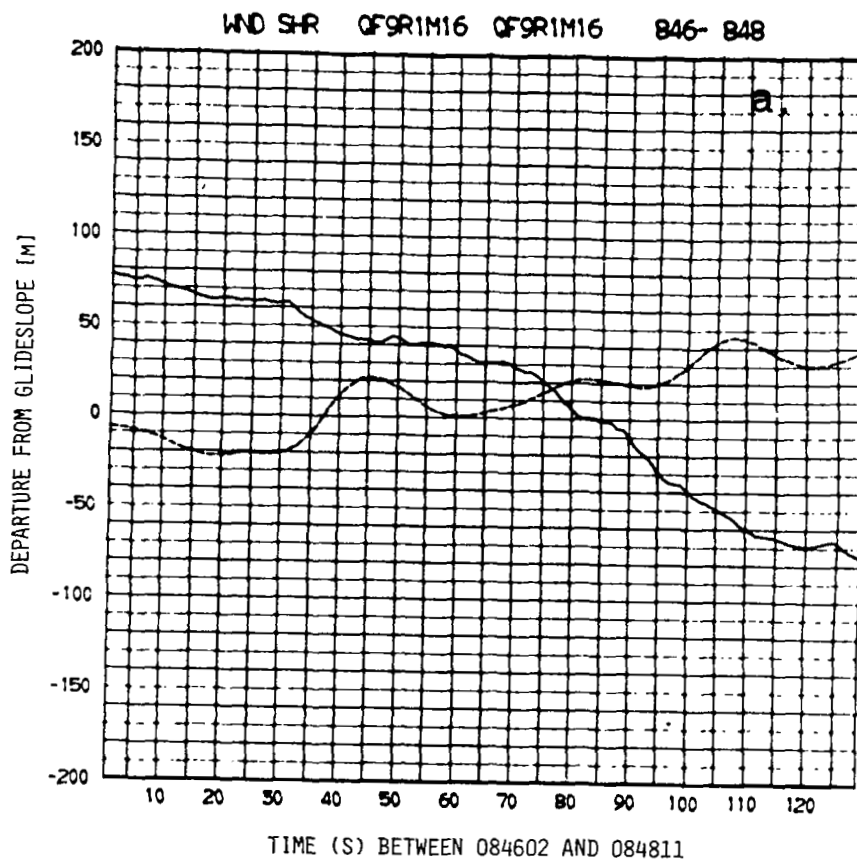
Figure 14a. QF9R1M16 showing aircraft (solid line) and model (dashed line) altitude (m) departure from a 3 deg glide slope path to the radar, with positive values representing altitude departures above the path, all as function of time.

53

WND SHR   QF9R1M16 QF9R1M16   846- 848
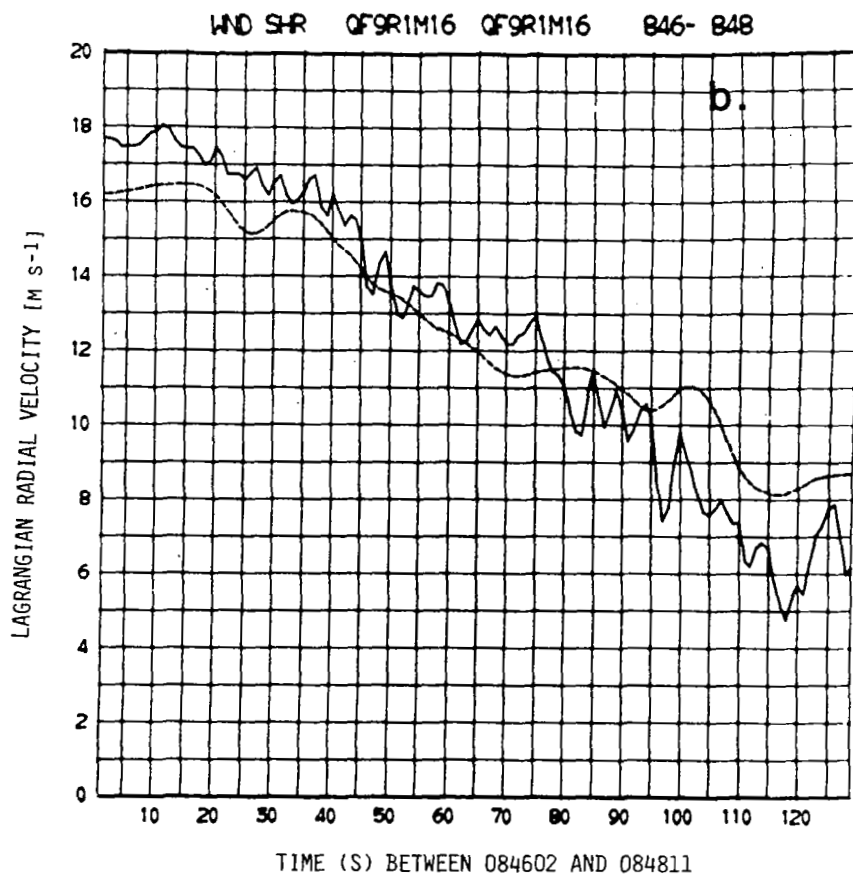
Figure 14b. QF9R1M16 comparison of aircraft (solid
line) longitudinal wind (m s^{-1}) and Lagrangian
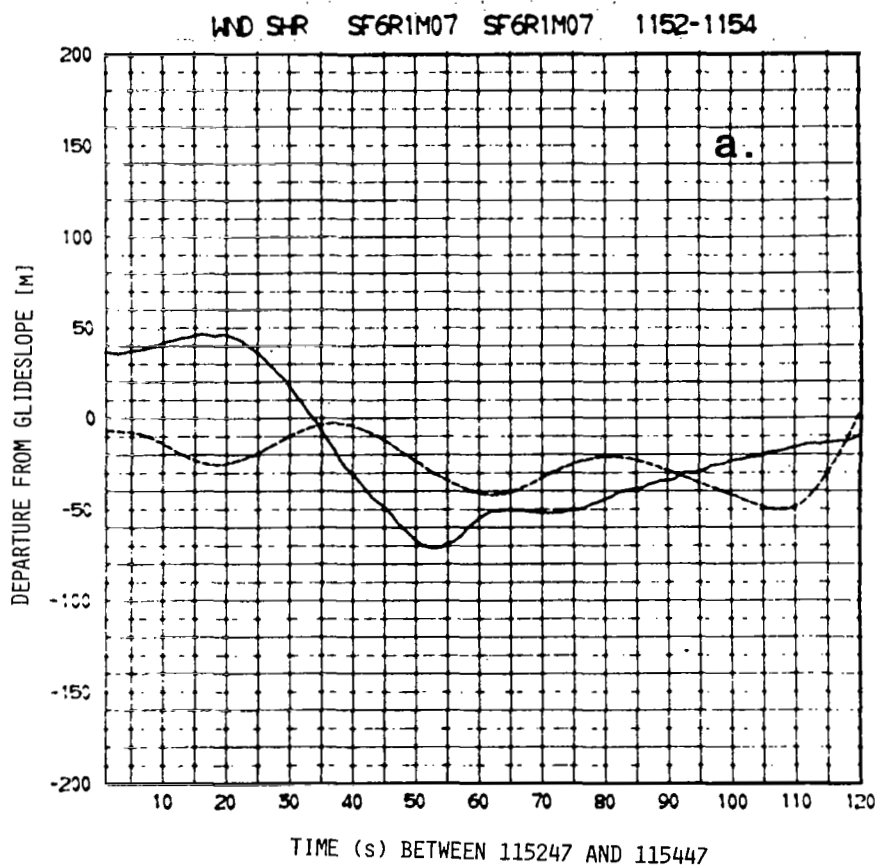Doppler velocity (m s^{-1}) (dashed line) as a function
of time.

54
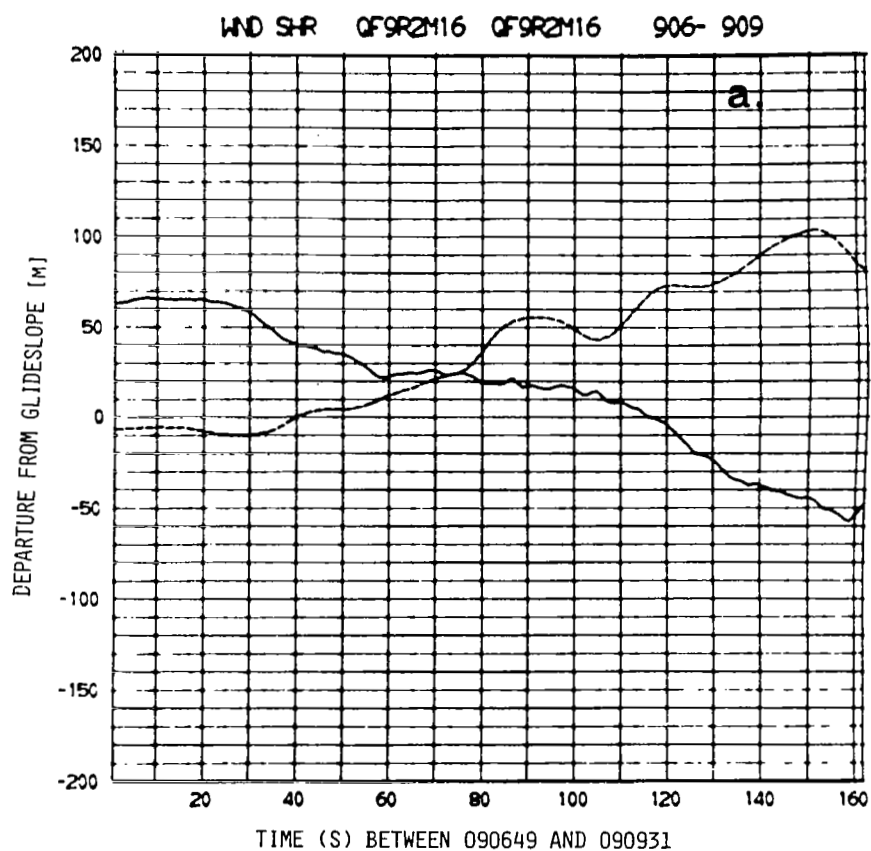
Figure 15a. QF9R2M16 showing aircraft (solid line)
and model (dashed line) altitude (m) departure from
a 3 deg glide slope path to the radar, with positive
values representing altitude departures above the
path, all as function of time.

WND SHR   QF9R2M16   QF9R2M16   906- 909

b.

LAGRANGIAN RADIAL VELOCITY [M s⁻¹]

TIME (S) BETWEEN 090649 AND 090931
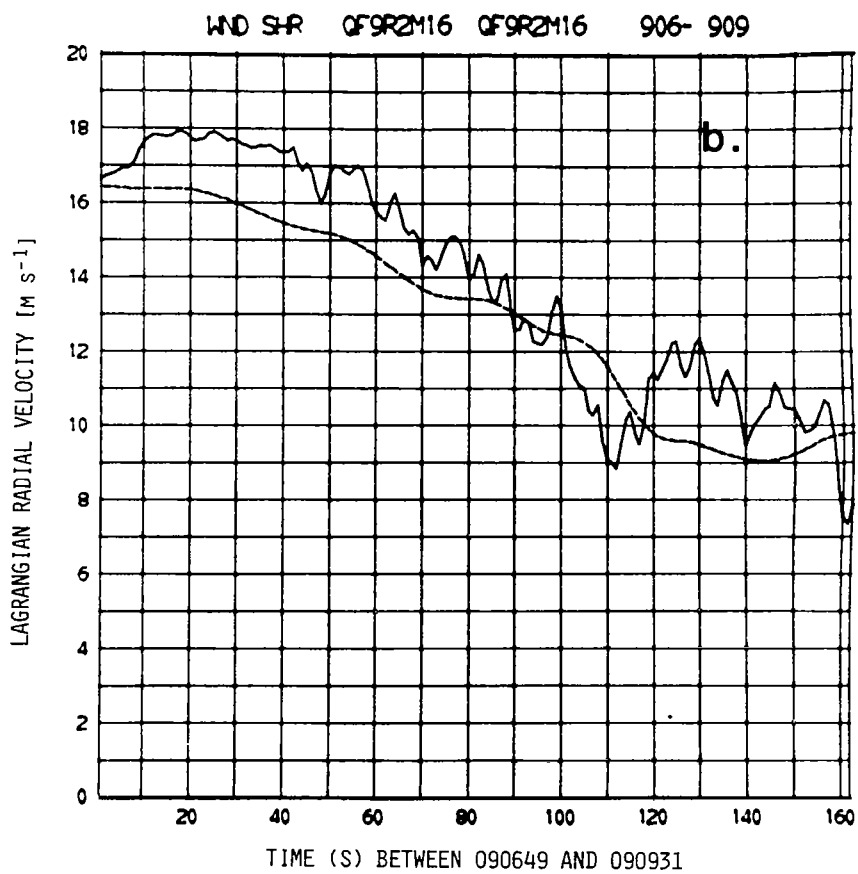
Figure 15b. QF9R2416 comparison of aircraft (solid line) longitudinal wind (m s⁻¹) and Lagrangian Doppler velocity (m s⁻¹) (dashed line) as a function of time.

a.

DEPARTURE FROM GLIDESLOPE [M]

200

150

100

50

0

-50

-100

-150

-200

20   40   60   80   100   120   140   160   180   200   220   240
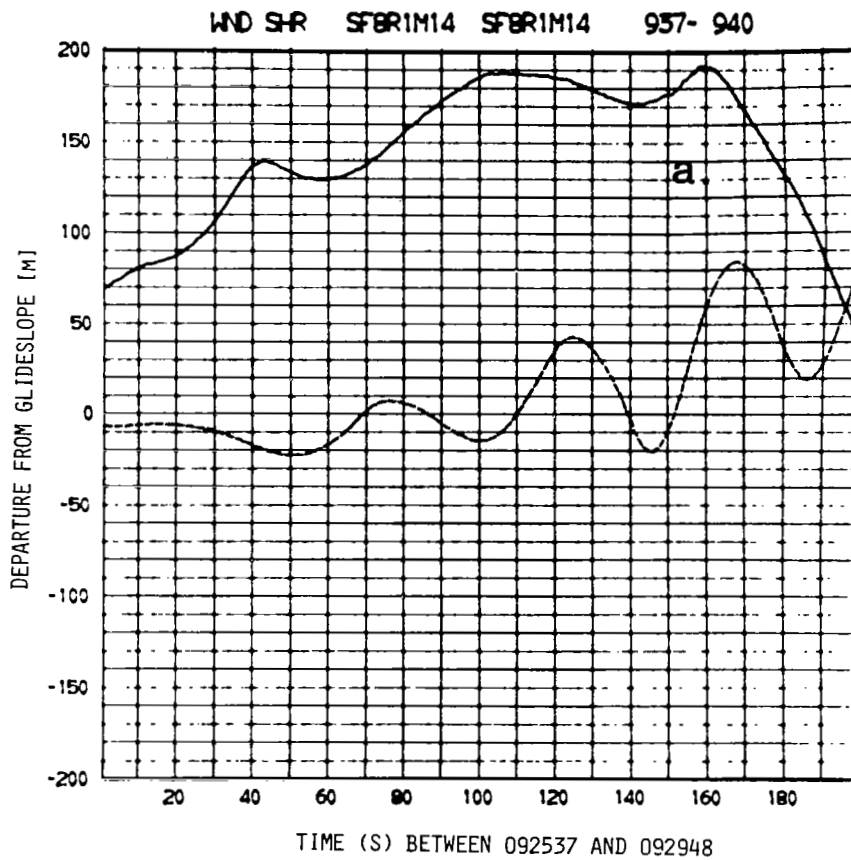
TIME (S) BETWEEN 085224 AND 085634
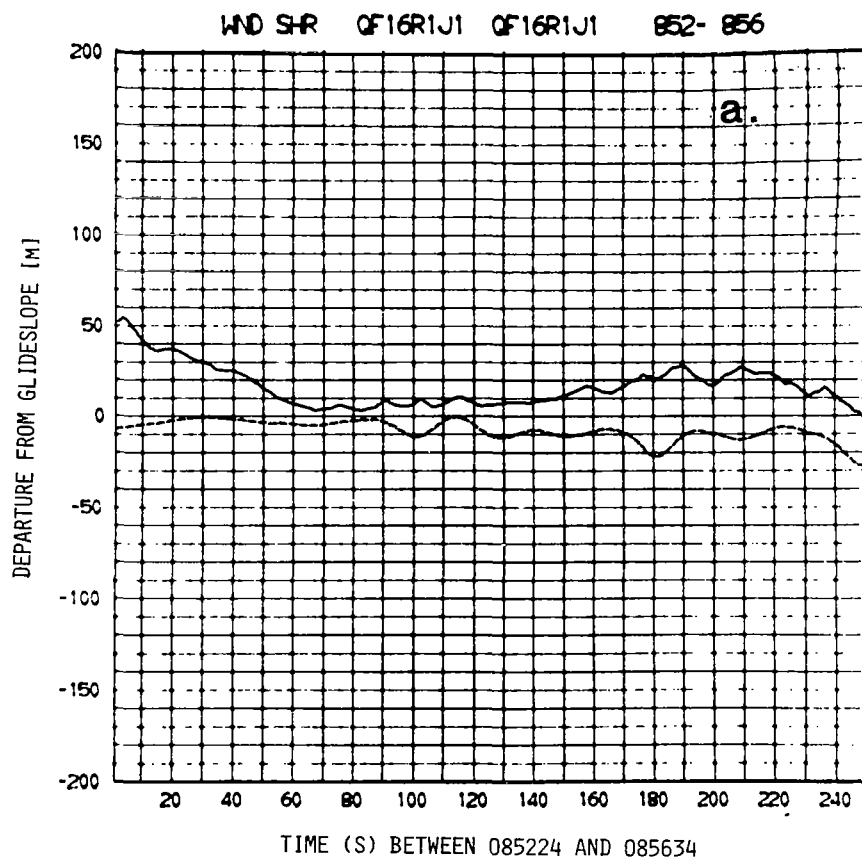
Figure 16a. QF16R1J1 showing aircraft (solid line) and model (dashed line) altitude (m) departure from a 3 deg glide slope path to the radar, with positive values representing altitude departures above the path, all as function of time.

57

WND SHR   QF16R1J1   QF16R1J1   852- 856

TIME (S) BETWEEN 085224 AND 085634
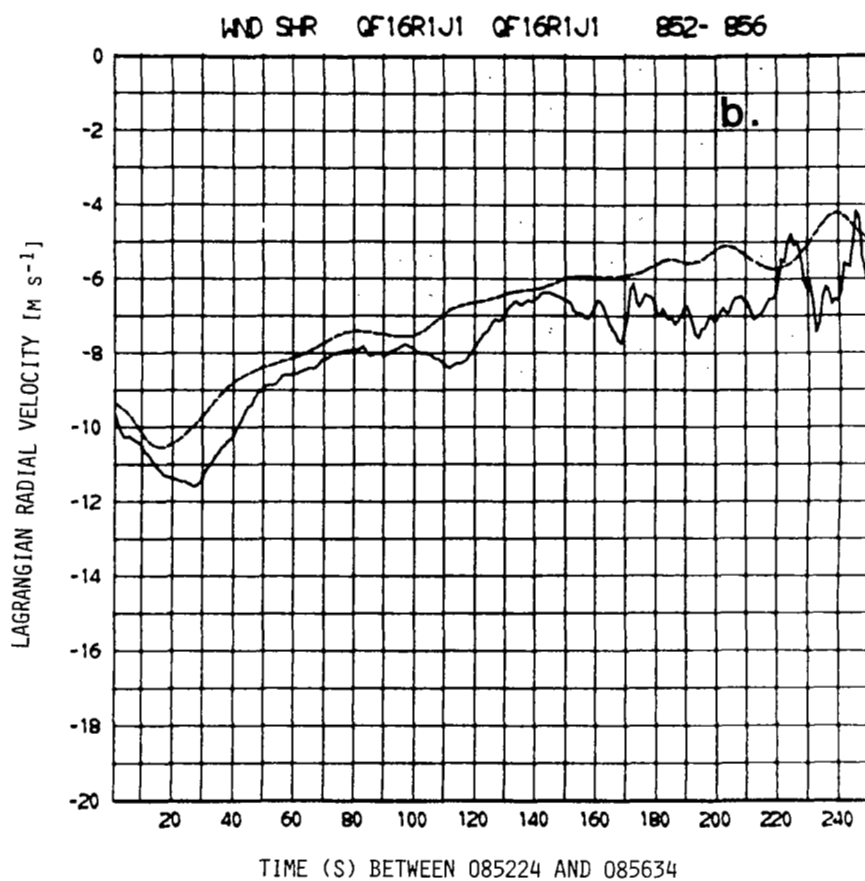
Figure 16b. QF16R1J1 comparison of aircraft (solid
line) longitudinal wind (m s^{-1}) and Lagrangian Doppler
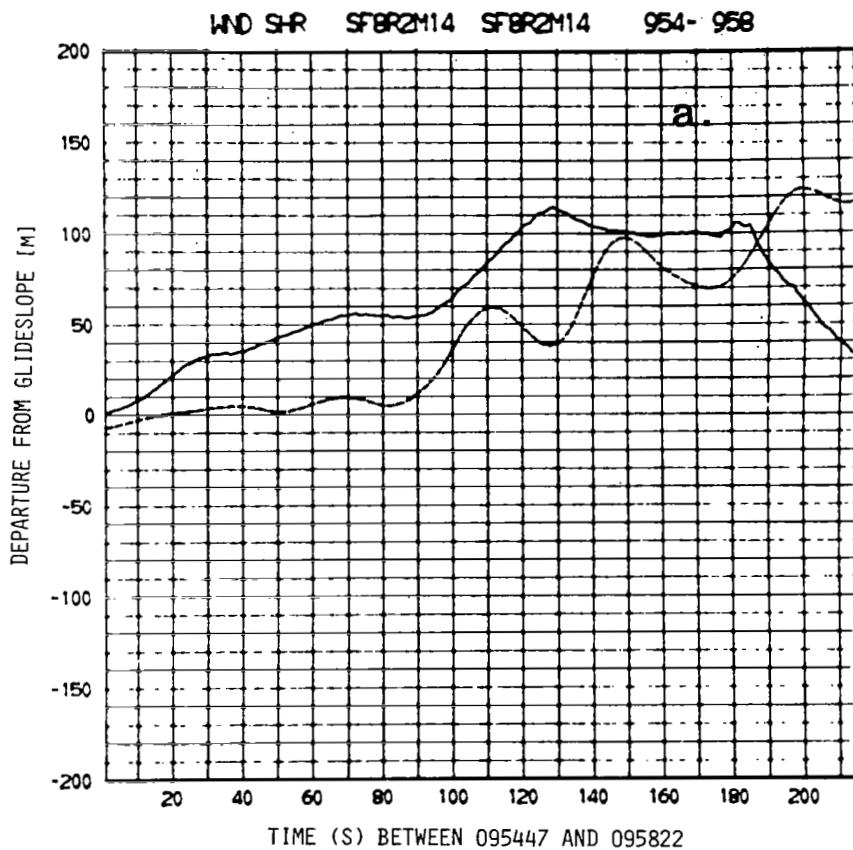velocity (m s^{-1}) (dashed line) as a function of time.

58
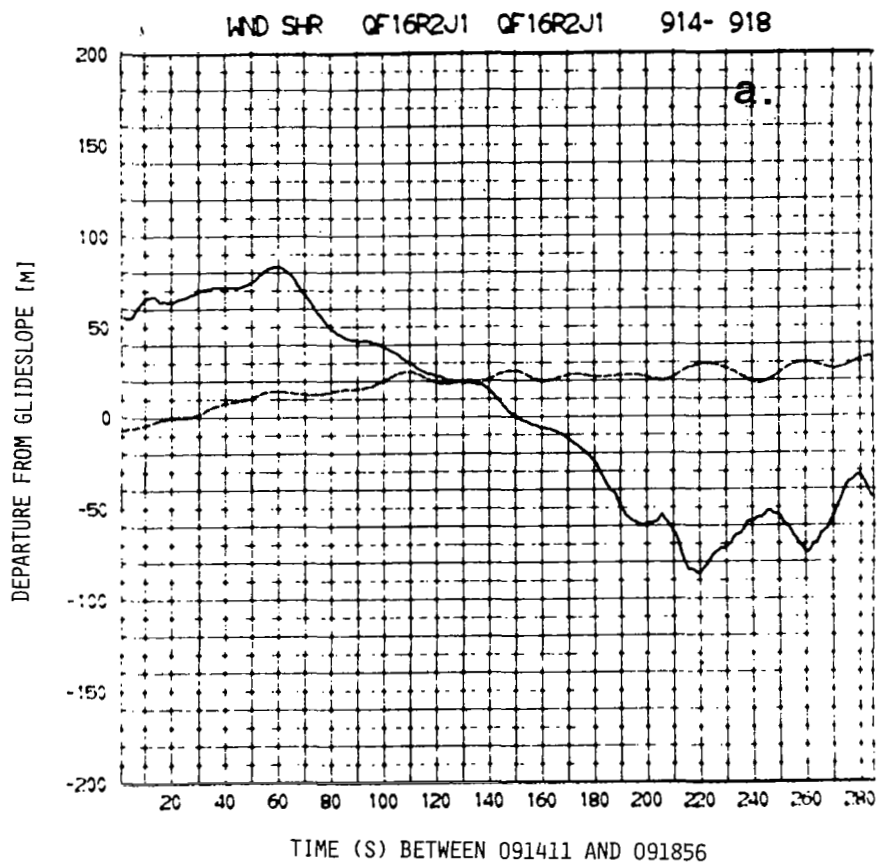
Figure 17a. QF16R2J1 showing aircraft (solid line) and model (dashed line) altitude (m) departure from a 3 deg glide slope path to the radar, with positive values representing altitude departures above the path, all as function of time.
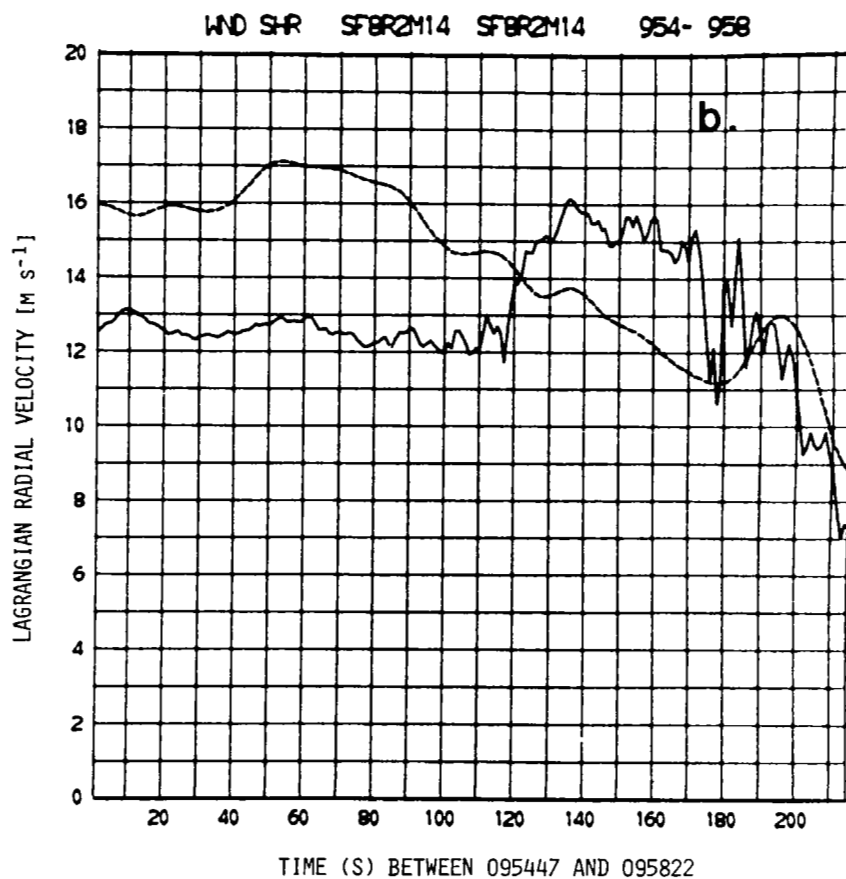
59

WND SHR   QF16R2J1   QF16R2J1   914- 918
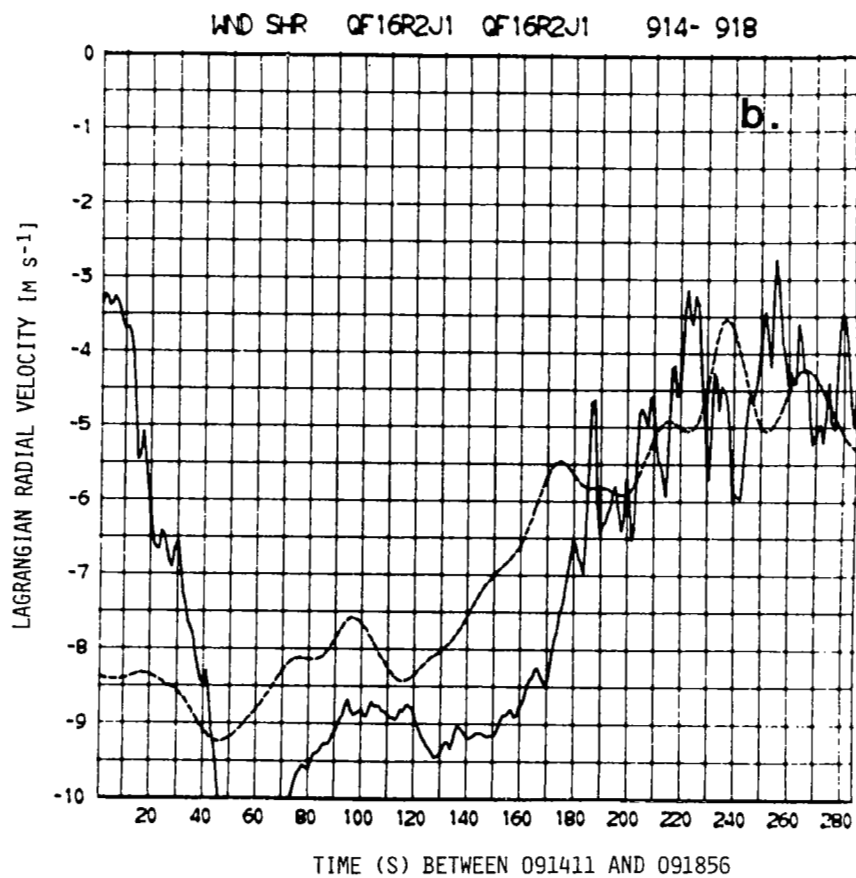
Figure 17b. QF16R2J1 comparison of aircraft (solid
line) longitudinal wind (m s⁻¹) and Lagrangian Doppler
velocity (m s⁻¹) (dashed line) as a function of time.

60

WND SHR QF17R2J4 QF17R2J4 1600-1602

a.

LAGRANGIAN RADIAL VELOCITY [M s⁻¹]

TIME (S) BETWEEN 160009 AND 160257
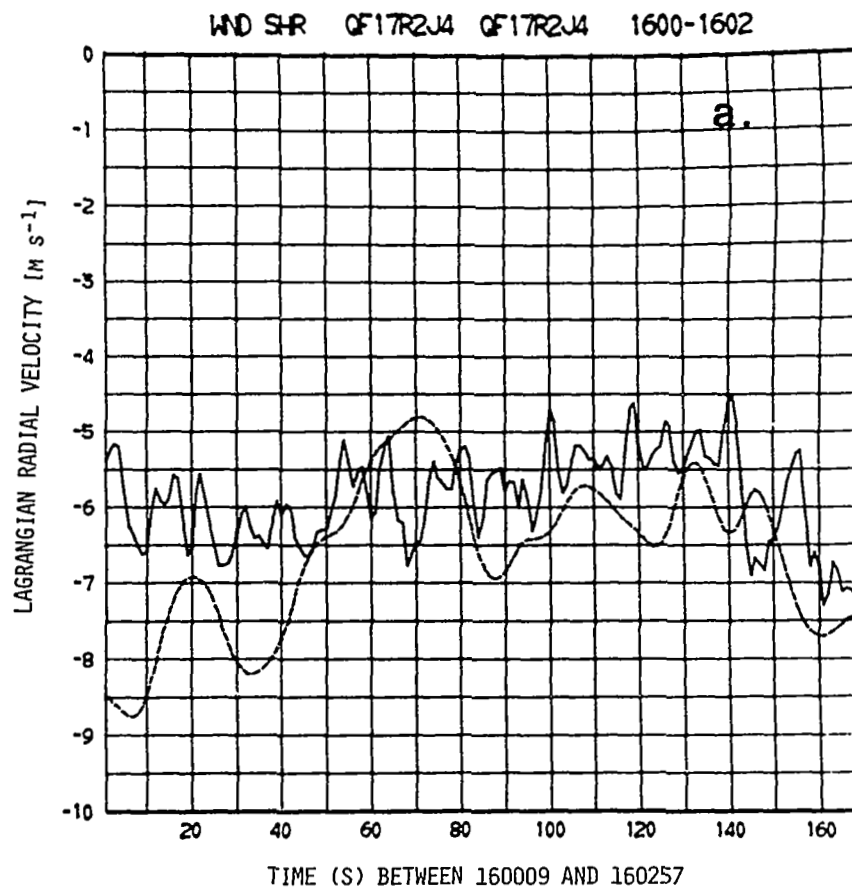
Figure 18a. QF17R2J4 comparison of aircraft (solid line) longitudinal wind (m s⁻¹) and Lagrangian Doppler velocity (m s⁻¹) (dashed line) as a function of time. NOTE: Altitude deviation data was not available.
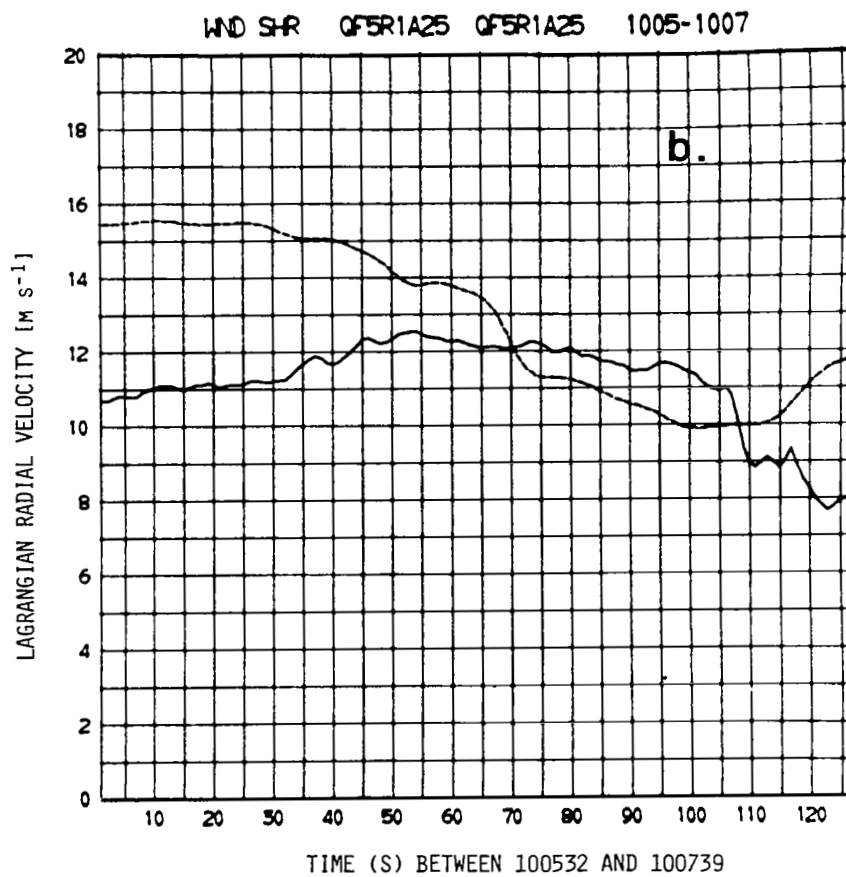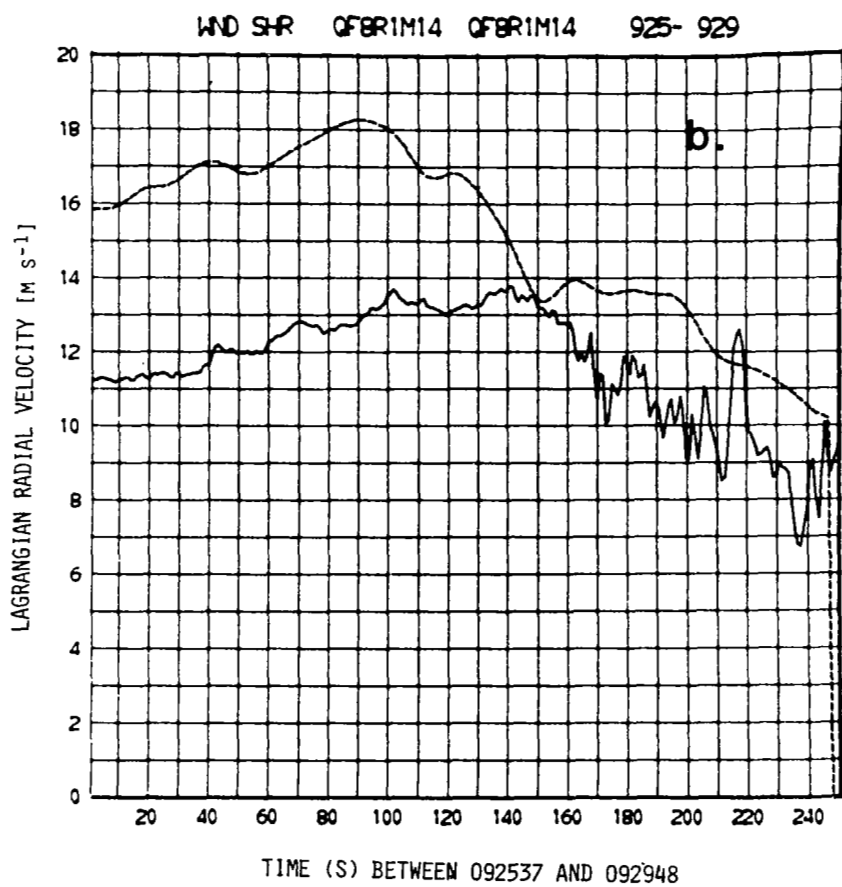
(1980), we believe Doppler scans on the order of once each minute might be required.

We were less pleased with the lack of phasing in the smaller scale features, particularly in 25% of our sample, as represented by case (b). We decided to look more carefully at the spectra which were used to obtain the Doppler wind profile, to see if a more satisfactory explanation could be obtained. Figure 19 represents ten such spectra, ranging from 9.55 to 8.2 km from the Norman radar. Although the spectra are not exactly clean, those at 8.2, 8.35, 8.5, and 9.55 km are single-moded, suggesting that our averaging technique using equations (1) and (2) was suitable. However, for the spectra at 8.65, 8.8, 8.95, 9.1, 9.25, and 9.40 km, a clear bimodal distribution is evident. Consequently, our radial velocity estimates at these latter ranges are probably inaccurate, a fact consistent with Figure 4f. The causes for such spectra are many, and there is no unique way to single out any one. For instance, strong point targets in the side lobes can spill enough power into contiguous range bins to create such spectra. Yet we cannot discard the possibility that meteorological signals on small scales are responsible for these bimodal velocity spectra. The presence of turbulent vortices or eddies, coupled with our lack of colocation in our comparisons, particularly in azimuth, could certainly account for some of the differences in aircraft and Doppler data. If the radar and aircraft sampling had been precisely colocated, we would expect these variations to be considerably less obvious. Finally, we know that even if this were the case, the two measurements differ in that the aircraft is providing a series of point velocity measurements, while the Doppler radar presents a reflectivity and resolution volume weighted mean values.
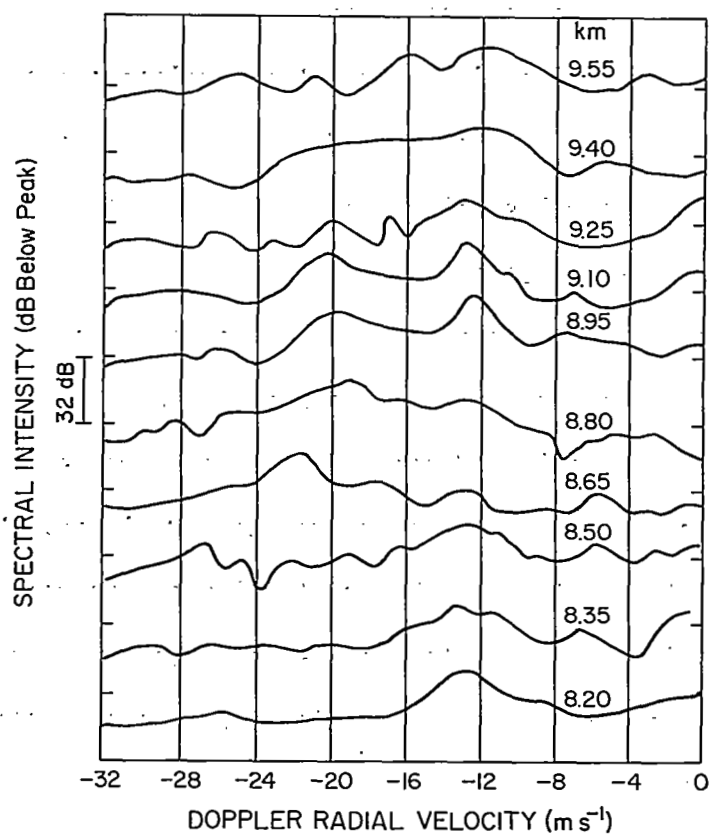
Figure 19. NSSL processor spectral display for
10 Doppler radial velocity spectra, ranging from
8.2 to 9.55 km, expressed as a function of spectral
intensity (dB below peak). For each spectrum dis-
played, three spectral data samples were averaged.
Time of sample was 114719 CST on 7 May 1979--refer
to Figure 4a-h for comparison.

The following conclusions are justified:

1. For 75% of the cases examined to date, excellent agreement is obtained.

2. Certain small-scale disturbances were not verified in the comparisons, due to the following problems:

   a. a lack of Doppler resolution,

   b. a lack of colocation of the two sampling systems,

   c. the possible presence of eddy or vortex-like disturbances within the pulse volume, as well as point targets in antenna side lobes.

3. If a Doppler radar were to obtain clear-air radial wind data precisely along the intended approach path, problems 2a and 2b would be greatly reduced. Furthermore, we believe that if the antenna was shrouded to reduce side lobes, the problem with point targets would be practically eliminated.

4. Use of a Doppler radar to provide the measurement component of an Airport Wind Shear Detection and Warning System appears justified.

CHAPTER IV

RESULTS OF FIXED STICK BLICK NUMERICAL SIMULATION MODEL

The model of aircraft performance developed by Blick, and reported
in McCarthy et al. (1979), was applied to the 16 approaches studied in
detail. Airplane transfer functions for the Queen Air and Sabreliner
were developed and tested. All model runs were made with the fixed stick
assumption, while a pilot-in-the-loop edition was run by Frost
and Turkel (1980). All runs were begun at the initial range indicated
in the figures of Chapter III, with the nominal airspeed for the Queen Air
and Sabreliner 61.77 m s^{-1} (120 knots) and 66.92 m s^{-1} (130 knots)
respectively. A typical example of the Blick model output is given in Figure 20.
As in McCarthy et al. (1979), we computed approach quality by two means:

$$\Delta u' = \left[\frac{1}{t_L} \int_0^{t_L} u^2 \, dt \right]^{1/2} \tag{8}$$

$$\Delta h' = \left[\frac{1}{t_L} \int_0^{t_L} (h - h_n)^2 \, dt \right]^{1/2} \tag{9}$$

Where $\Delta u'$ is the root-mean-square value of airspeed (m s^{-1}) deviation
from the nominal or equilibrium airspeed, $\Delta h'$ is the root-mean-square
value of altitude deviation from the 3 deg glide slope, t_L is the total
approach time (s) to landing, u is airspeed (m s^{-1}), h is aircraft alti-
tude (m), h_n is nominal aircraft altitude (m) along a 3 deg glide slope,
and t is time (s). From the equations and as discussed in McCarthy et al.
(1979), we can see that large values of $\Delta u'$ and $\Delta h'$ represent serious
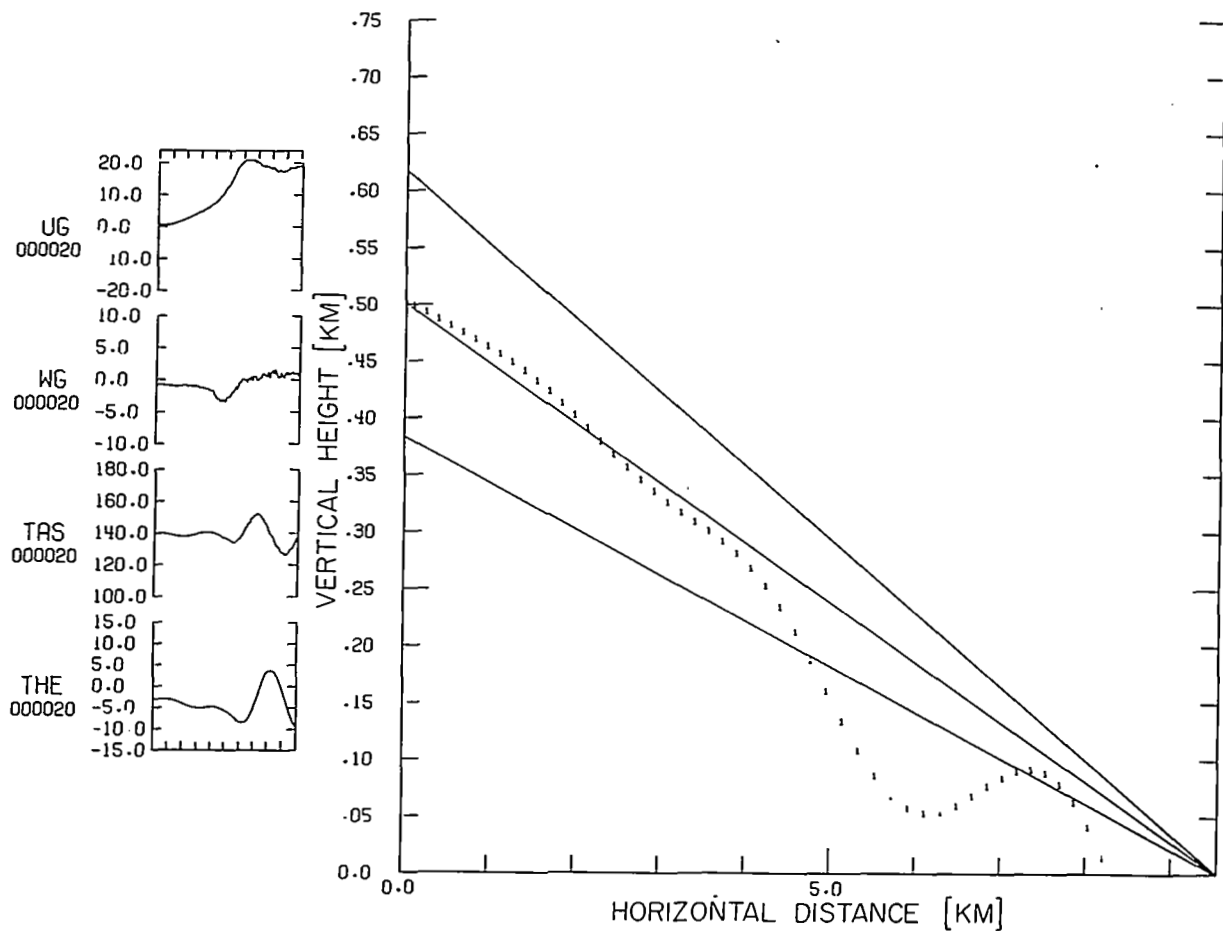
Figure 20. Typical input and output of Blick model.
Case is for Boeing 727 airplane. Input, shown as
top two panels on left, are horizontal (UG) and
vertical (WG) wind; output are true airspeed (TAS)
and pitch angle (THE). Trace shows glide slope and
0.7 deg missed approach limits (solid lines) and
aircraft position (1's).

66

deteriorations of the approach. Consequently, we call $\Delta u'$ and $\Delta h'$ approach deterioration parameters (ADP).

To gain further insight into the importance of the horizontal phugoid wave, we have examined the approach deterioration parameters of a B-727 class airplane, when full, half, and one-quarter sinewaves of horizontal (longitudinal) winds, precisely at the airplane's phugoid frequency, are inputted into the controlled-fixed simulation model. Results are shown in Table 2 in terms of $\Delta u'$, $\Delta h'$, and DTD; here DTD represents the distance long or short of aircraft nominal touchdown. Our work suggests that $\Delta u'$ may be the most useful indicator, since airspeed fluctuations may be the most difficult for the pilot and airplane to handle. Note that the $\Delta u'$ parameter is rms velocity, and not the instantaneous airspeed. It is clear that an aircraft encounter with a full wave can be most serious, as can the half wave situation. The one-fourth wave situation, representing a simple ramp or step shear which may be encountered in a gust front, is considerably less serious than an encounter with a phugoidal wave. Another interesting point is seen when the ADP values for Eastern Air Lines Flight 66, as reported in McCarthy et al. (1979), are considered in the context of Table 2. Notice that this crash occurred when the airplane encountered a relatively low 1/2 wave amplitude. Recent studies of the phugoidal waves associated with severe thunderstorms show amplitudes in the 15 to 25 m s^{-1} range (see Wilson et al., 1980), and implies that the Eastern Flight 66 of wind shear accident may be associated with relatively non-severe storms, a fact well documented by Fujita and Caracena (1977). Pilots have long avoided severe thunderstorms; this work shows the extreme danger associated with weak thunderstorms that have phugoidal waves.

TABLE 2

Approach deterioration parameters for Boeing 727 class airplane, for simulated sinusoidal full, half and one-fourth wave longitudinal wind inputs at airplane phugoid frequency of 0.026 Hz, for control-fixed model, with both initial headwind and initial tailwind cases, for 5, 10, 15, 20, m s^{-1} amplitudes. DTD (km) is airplane touchdown distance from nominal (runway), with negative being short, positive long.*

		Initial Headwind				Initial Tailwind			
		Wave Amplitude (m s^{-1})							
		5	10	15	20	20	15	10	5
$\Delta u'$	Full Wave	4.8	10.2	16.6	23.9	23.0	16.0	9.9	4.7
	Half Wave	2.3*	4.6	6.9	9.3	9.8	7.3	4.7	2.3
	One-Fourth Wave	1.5	3.0	4.6	6.1	7.5	5.2	3.4	1.6
$\Delta h'$	Full Wave	47.6	129.6	237.5	350.4	318.6	209.1	109.0	39.5
	Half Wave	17.0*	36.1	61.5	95.2	139.3	90.7	52.1	22.2
	One-Fourth Wave	32.2	57.8	75.3	85.0	212.2	149.6	93.5	43.3
DTD	Full Wave	-0.93	-3.39	-6.65	-9.98	-9.26	-5.95	-2.78	-0.40
	Half Wave	+0.01	-0.17	-1.02*	-2.16	-2.27	-1.87	-0.72	-0.17
	One-Fourth Wave	+0.53	+1.01	+1.30	+1.36	-4.57	-2.59	-1.91	-0.89

*Represents approximate values for Eastern Air Lines Flight 66.

68

Table 3 gives $\Delta u'$ and $\Delta h'$ for our 16 simulations. Shown are values for the Lagrangian and two Eulerian estimates, as defined in Chapter III. The most obvious feature seen in the table is the absence of large values of model output $\Delta u'$ and $\Delta h'$. This is particularly true for $\Delta u'$, where rms airspeed variations (Eulerian Before--1 sec before test) from nominal never exceed 2.1 m s^{-1}, with the average being only 1.0 m s^{-1}. Remember that the Eastern Air Lines Flight 66 value was 3.5 m s^{-1}. Note too, that the Sabreliner average is 2.0 m s^{-1} while the Queen Air average is 0.7 m s^{-1}. The Sabreliner has a higher phugoidal response than does the Queen Air, as may be suggested in these data.

With regard to $\Delta h'$, for a fixed stick model, certain altitude departures from the glide slope readily can be corrected were pilot controls included. Consequently less importance is attached to $\Delta h'$ values. More discussion of this point can be found in McCarthy et al. (1979).

We have plotted the results of the Blick output as a dashed line on Figure 3a-e, 4a-e, and 5 to 18, for the Eulerian Before case (1 sec after test). Results are quite similar for the Eulerian After and Lagrangian and consequently are not shown.

It is clear from Table 3 and the plotted figures that we did not encounter significantly adverse wind shear. We attribute this to the fact that our pilots, controllers, and SESAME '79 Aircraft Coordinator[1] did not want to attempt PAR approaches in dangerous wind shear conditions. This serious limitation in the planned test of feasibility will be discussed in detail in Chapter VII.

---

[1]Lead author, John McCarthy.

TABLE 3

Approach deterioration parameters (ADP, Δu' and Δh') for 16 Blick Fixed stick simulations. Also include ADP are estimates of actual aircraft performance, to be discussed in Chapter VI.

Approach Code	$\Delta u'$ Lagrangian	$\Delta u'$ Eulerian Before	$\Delta u'$ Eulerian After	$\Delta u'$ Aircraft	$\Delta h'$ Lagrangian	$\Delta h'$ Eulerian Before	$\Delta h'$ Eulerian After	$\Delta h'$ Aircraft
	$m\ s^{-1}$	$m\ s^{-1}$	$m\ s^{-1}$	$m\ s^{-1}$	m	m	m	m
SF6R1M07	2.1	2.6	1.3	1.9	20.3	24.8	15.7	40.6
SF8R1M14	0.7	2.4	1.0	4.8	29.7	37.6	28.7	149.2
SF8R2M14	1.6	1.4	2.0	7.2	36.0	34.7	33.3	73.4
SF8R3M14	2.1	1.4	1.4	2.4	20.9	16.3	16.3	108.4
QF5R1A25	0.4	0.5	0.5	1.4	25.3	23.6	25.6	75.6
QF5R3A25	0.4	0.5	0.8	3.2	10.9	13.4	29.7	32.2
QF7R3M07	0.8	1.0	1.1	2.9	9.1	7.6	15.2	69.6
QF8R1M14	0.5	0.7	0.6	3.8	23.5	26.6	24.8	69.9
QF8R2M14	0.7	0.7	0.6	3.0	27.1	20.5	24.3	74.4
QF8R3M14	0.4	0.7	0.8	4.5	24.8	22.3	26.0	41.5
QF9R1M16	0.3	0.9	1.0	1.7	36.9	39.1	46.1	51.3
QF9R2M16	0.4	0.8	0.8	4.8	46.7	35.9	40.6	39.3
QF9R3M16	0.4	0.8	1.0	4.9	19.9	39.3	47.0	71.7
QF16R1J1	0.5	0.6	0.6	2.9	15.6	26.2	26.2	20.3
QF16R2J1	0.8	0.4	0.5	4.2	12.9	13.9	13.1	54.0
QF17R2J4	0.8	0.9	0.8	1.7	9.1	13.2	11.5	18.7

CHAPTER V

PAR APPROACH QUALITY ASSESSMENT TOOL

As an independent method of assessing the quality of the approach, an approach quality assessment tool, designed to be completed by the pilot, was developed by Mr. A. L. Fincher. Figure 21 is a copy of this evaluation sheet. Table 4 presents the results of its use for 15 of the 16 approaches studied (the evaluation for Sabreliner Flight 6 Run 1 was not available). As a means of estimating the quality of the approach, we have totalled questions 7 through 12, by assigning a numerical value of 1 for a, 2 for b, and 3 for c. These totals indicate that Queen Air approaches 16-2, 9-3, 8-3, and 5-3 were considered by the pilots to be the most adverse. However, as is clear from the last chapter, none of our approaches were conducted in truly dangerous shear conditions. We believe, however, that the usefulness of this tool will be more meaningful in an experiment where a greater range of shear is encountered.

Date _____

Pilot's Name _____

Aircraft I.D. _____

Approach Start Time _____

Approach Stop Time _____

APPROACH QUALITY
(PILOT)

1. Approximately how many power adjustments were required on this approach?

   a. Less than five (5)
   b. More than five (5) but less than ten (10)
   c. More than ten (10)

2. Concerning the magnitude of power changes; In your opinion, were the power adjustments required on this approach?

   a. Only minor
   b. Moderate
   c. Major Power Corrections

3. Approximately how many pitch adjustments were required on this approach?

   a. Less than five (5)
   b. More than five (5) but less than ten (10)
   c. More than ten (10)

4. Pitch corrections on this approach were:

   a. Slight and predominantly less than five (5) degrees.
   b. Moderate - between five (5) and ten (10) degrees.
   c. Significant - more than ten (10) degrees.

5. Concerning azimuthal deviations from the final approach course, on this approach there were:

   a. Only "minor" deviations
   b. Significant deviations
   c. Extreme deviations

6. Concerning vertical deviations from the glide path on this approach, there were:

   a. Minor deviations
   b. Significant deviations·
   c. Extreme deviations

Figure 21a. Pilot approach quality assessment evaluation form, questions 1 through 6.

7. Turbulence experienced on this approach could be catego-
   rized as:

   a. None
   b. Light
   c. Moderate
   d. Severe

8. Airspeed deviations on this approach were:

   a. Less than five (5) knots
   b. More than five (5) knots
   c. More than ten (10) knots

9. Maximum changes in vertical velocity (VVI) indications re-
   quired to fly this approach were:

   a. 250 FPM or less
   b. More than 250 FPM but less than 500 FPM
   c. More than 500 FPM

10. How would you evaluate the final controller's performance
    on this approach?

    a. Excellent
    b. Average
    c. Below average

11. How would you characterize the "safety" of this approach?

    a. Completely safe
    b. Marginally safe
    c. Unsafe

12. What was your "overall impression" of this approach?

    a. Easily flown, only minor inflight deviations, and com-
       pletely safe.
    b. Required a good deal of concentration with some inflight
       deviations.
    c. Required significant concentration and above average
       piloting skills to successfully complete the approach.

 Please add any additional pertinent comments:

     Figure 21b.   Questions 7 through 12.

73

TABLE 4

Summary of Approach Quality Assessment Tool

Approach Code	Question						Total
	7	8	9	10	11	12	
SF6R1M07	------------------N/A----------------------------						
SF8R1M14	1	1	1	1	1	1	6
SF8R2M14	2	1	3	2	1	1	10
SF8R3M14	2	1	1	2	1	1	8
QF5R1A25	2	1	3	1	1	1	9
QF5R3A25	2	2	2	1	3	2	12
QF7R3M07	3	1	1	1	1	1	8
QF8R1M14	2	1	2	1	1	1	8
QF8R2M14	2	2	2	1	1	1	9
QF8R3M14	2	2	2	1	3	2	12
QF9R1M16	2	2	2	1	1	1	9
QF9R2M16	2	1	2	1	1	1	8
QF9R3M16	2	3	3	1	3	2	14
QF16R1J1	2	2	1	1	1	1	8
QF16R2J2	2	3	3	1	3	2	14
QF17R2J4	2	2	1	1	1	1	8

CHAPTER VI

COMPARISON OF AIRCRAFT PREDICTED RESPONSE

TO ACTUAL AIRCRAFT RESPONSE

A major objective of this feasibility study was to test the ability of our numerical simulation model to predict actual aircraft performance on the PAR approach course. The sequence of this prediction is illustrated in Figure 22, which depicts our concept of a real-time detection and warning system, as previously presented in McCarthy et al. (1980a). In the real-time concept, we would derive an approach deterioration parameter by using a Doppler wind profile which approximates our Eulerian Before profile used in this feasibility study. Decisions by the air traffic controller, or by the pilot, with the ADP data uplinked to the cockpit, would be made prior to executing an approach.

In our study, we had the benefit of comparing predicted performance to that actually encountered by the instrumented aircraft. Table 3 gives the results of model (or predicted) approach parameters, as well as a calculation of actual aircraft values. All calculations used equations (8) and (9). An independent assessment of the approach quality was obtained from the pilot evaluation tool, as given in Figure 21 and Table 4.

As is obvious from the discussions in the preceding two chapters, essentially all of our approaches were conducted in weak shear conditions. This is seen clearly when model-derived ADP values of Table 3 are compared to much more intense shear, seen in the theoretical values given in Table 2. However, actual aircraft ADP values are considerably higher
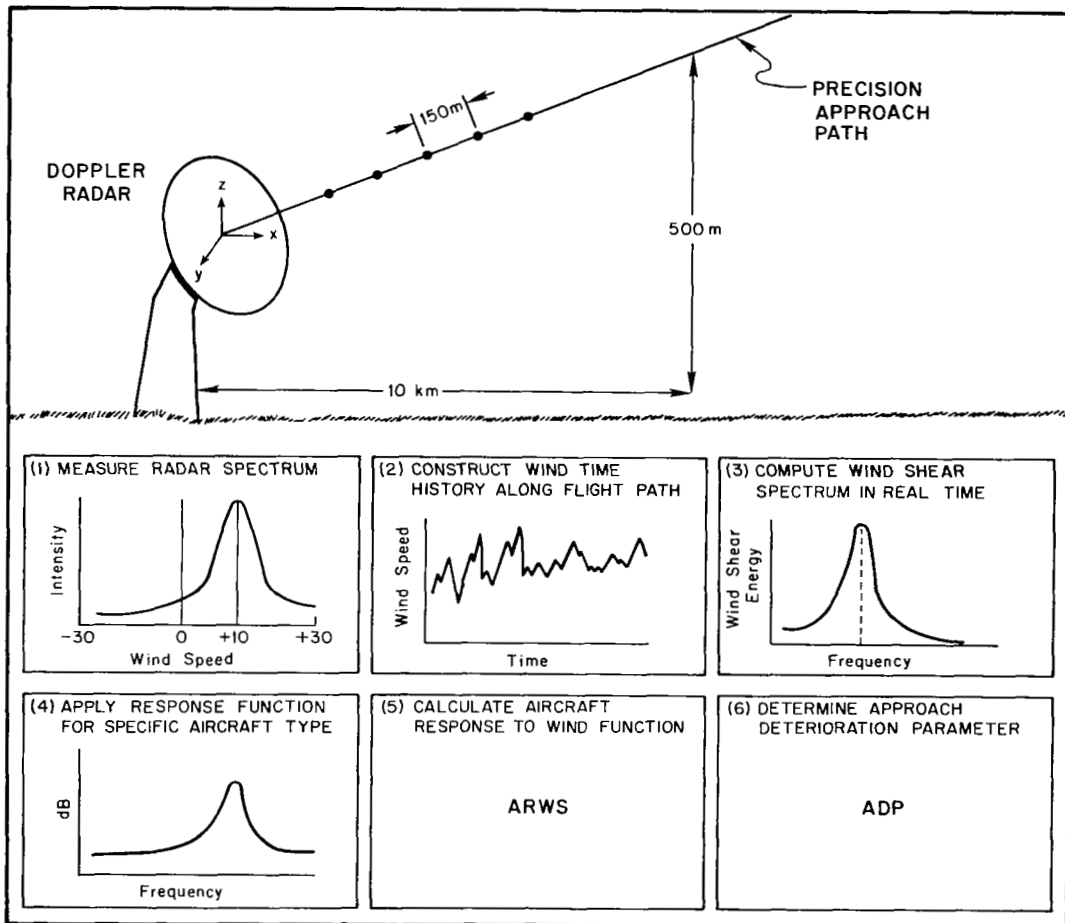
Figure 22. Diagrammatic illustration of wind shear detection and warning system. Process is sequential, starting from Doppler radar measurement of winds along the precision approach path, and ending with a prediction of approach deterioration for a particular class of airplane. In a real-time system, steps 1-6 would take place within several seconds by use of a computer slaved to the Doppler.

than model estimates. This discrepancy may be due to imprecision in vectoring our SESAME aircraft precisely onto the PAR course. Furthermore it was not always possible to maintain a fixed stick mode, due to traffic, shear conditions, and controller instructions.

Inspection of Table 3 for an estimate of the prediction skill of the Blick model gives the impression of a rather inadequate capability. More specifically, we are testing the $\Delta u'$ or $\Delta h'$ ADP for the Eulerian Before case as a predictor of the $\Delta u'$ and $\Delta h'$ for the real Aircraft data results case. We find the case for a good predictive ability less than convincing.

To examine the predictive ability further, we computed linear regressions, where the independent variable was the actual aircraft response, and the dependent variable was the Blick model response. The results are given in Table 5. Actual values of $\Delta u'$ and $\Delta h'$ approach deterioration parameters were taken from Table 3. Some rather interesting but tenuous conclusions can be drawn. First of all, when all 16 approaches are included, no significant correlations result (Case a); the same holds true when just Queen Air approaches are considered (Case b). We see a little more correlation when only the Sabreliner approaches are examined (Case c). Surprisingly the altitude variation ADP, $\Delta h'$, appears to be better correlated than $\Delta u'$. However, as in our earlier inspection, the most obvious conclusion is that actual aircraft approach deterioration parameters are not well correlated to model predictions.

We tried one additional correlation to see if our independent approach quality assessment, discussed in Chapter V, could provide a means of stratifying the more adverse wind shear situations. In Table 5, Case (d) represents the correlation between model predicted and actual

77

TABLE 5

Linear regression slope, intercept, correlation coefficient, and explained variance for $\Delta u'$ and $\Delta h'$ ADP values, for four tests: (a) all 16 approaches, (b) for 12 Queen Air approaches, (c) for 4 Sabreliner approaches, and (d), for the four most adverse approaches identified in Table 4 as QF16R2J1, QF9R3M16, QF8R3M14, and QF5R3A25.

Case	Variable	Aircraft	Sample Number	Slope	Y-Intercept	Linear Correlation Coefficient	Explained Variance (%)
(a)	$\Delta u'$	S/QA	16	0.03	0.93	0.00	6
	$\Delta h'$			0.08	19.79	0.07	26
(b)	$\Delta u'$	QA	12	-0.02	0.76	0.01	11
	$\Delta h'$			0.06	20.24	0.02	12
(c)	$\Delta u'$	S	4	-0.11	2.38	0.16	40
	$\Delta h'$			0.06	22.71	0.08	29
(d)	$\Delta u'$	QA/most adverse	4	0.17	-0.12	0.46	68
	$\Delta h'$			0.56	-5.87	0.63	80

aircraft ADP values. In this case the correlations seem to approach significant values, with 68% and 80% of the variance explained between predicted and verified values of $\Delta u'$ and $\Delta h'$, respectively.

We do not want to overemphasize the importance of these simple stratifications. However, we might draw the following conclusions:

1. Most of the approaches were made through weak wind shear.

2. For the total sample of 16 approaches, which are heavily weighed toward weak shear situations, the Blick fixed stick model does a poor job of predicting aircraft performance. Looking at it another way, the atmospheric shear signal and the aircraft response, when examined by the model, are in the "noise," where presumably other factors such as occasional pilot hands-on periods, moments of aircraft being out of trim, inadequacies of the Doppler radar wind measuring system, etc., cause errors in the predictive abilities of the model.

3. The capabilities of the model to predict the response of the Sabreliner somewhat more accurately may lie in the fact that this aircraft is more sensitive to changes in the wind than is the Queen Air.

4. As the atmospheric signal contains more shear, and hence has a more deleterious effect on aircraft performance, the model's capability to predict aircraft performance is enhanced. Or in other words, the strength of the shear brings the model predictive power out of the "noise."

CHAPTER VII

CONCLUSIONS

1. Summary and Overall Assessment

A feasibility study was conducted to determine whether ground-based Doppler radar could measure the wind along the path of an approaching aircraft with sufficient accuracy to be used to predict aircraft performance. A severe storm research program, SESAME '79, provided the tools for this test, including two instrumented research aircraft, a Sabreliner and Queen Air from NCAR, a Doppler radar at NSSL, and an Air Force PAR unit for precision approaches to the Doppler radar.

Forty-three PAR approaches were conducted, with 16 examined in detail. In each, Doppler-derived longitudinal winds were compared to aircraft measured winds; we concluded that in approximately 75% of the cases, the Doppler and aircraft winds were in acceptable agreement. In the remaining cases, errors may have been due to a lack of Doppler resolution, a lack of colocation of the two sampling volumes, the presence of eddy or vortex-like disturbances within the pulse volume, or the presence of point targets in antenna side lobes. It was further concluded that shrouding techniques would have reduced the side lobe problem. The work left little doubt that a ground-based Doppler radar, operating in the optically clear air, would provide the appropriate longitudinal winds along an aircraft's intended flight path.

The study went on to attempt to test whether, given the winds along the intended approach path taken immediately prior to the start

81

of an approach, a fixed stick numerical simulation model could predict aircraft performance. We found that most of our cases occurred in extremely weak wind shear conditions, and the resulting model calculation was unable to quantify precisely the aircraft performance, in terms of shear conditions. However, for the four approaches identified by an independent quantitative pilot assessment, the model was more successful. This led to the conclusion that as the shear became more severe, the model's capability improved. However, we were not able to verify this in a convincing manner. Finally, we obtained some field indications that a high performance jet transport (Sabreliner) was more adversely affected by shear than was a light piston transport (Queen Air), presumably operating in similar conditions.

2. Preliminary Plans for an Experiment With Aircraft Flight Simulators

In our feasibility study we were unable to encounter shear of a magnitude to cause a major effect on our aircraft performances, due to our unwillingness to endanger our crews and equipment. This was fortunate for our crews, but unfortunate for an adequate test of the concept. We now believe that any subsequent field test of wind shear detection and warning should always avoid intentionally placing aircraft in even remotely dangerous situations. Consequently we believe that the final "calibration" of the theoretical results given in McCarthy et al. (1979) must be conducted in manned aircraft flight simulators. Shears covering a range of wavelengths and profiles, both those measured in the atmosphere and the theoretical ones such as those given in Table 2, can be studied with real pilots manning flight simulators such as the Boeing 727, 747, L-1011, and DC-10.

We have had preliminary discussions with one airline regarding a possible operational/experimental program. We believe that a full flight simulator program with an air carrier would be both beneficial to our work, and to the air carrier, providing pilots with experience in encountering wind shear containing high energy at the phugoidal wavelength. We will continue to pursue the establishment of a program with an air carrier. Anticipating such an arrangement, we will be identifying and refining appropriate wind shear profiles, and preparing them in the correct format for input into flight simulators.

3. Preliminary Plans For a Field Experiment In 1982

As we discussed in Chapter I, several concepts regarding wind shear and its detection and warning have been advanced. To identify gust front and other singularities, the low level wind shear alert and microbarograph systems have been developed. To measure actual shear along a quasihorizontal approach or departure path, groups represented by McCarthy and Offi have investigated ground-based Doppler radar techniques and Tinsley (FAA) has called for airborne systems utilizing the airspeed/groundspeed difference technique. Finally, Fujita has identified the downburst mechanism, but has not established a technique for their real-time detection and warning.

We propose that a major field program be planned and executed, possibly during the summer of 1982, at Denver's Stapleton Airport. We envisage this program to be a test of the existing and anticipated technology designed to detect and warn of wind shear. By that time the FAA's operational wind shear program will have in place at Stapleton the

83

low-level wind shear alert (already in place) and microbaragraph systems.
NCAR's 5 and 10-cm Doppler radars could be made available on request, as
could PAM I and/or PAM II surface mesonet systems, and several instrumented
research aircraft. Mesoscale observing and display systems of the
Prototype Regional Observing and Forecast System (PROFS) of NOAA may be
available, and remote probing techniques of NOAA's Wave Propagation
Laboratory would be important. One or more air carriers with major
operations at Stapleton could be stimulated into participating. Finally
it is anticipated that the FAA will have prototype airborne wind shear
detection systems available for testing by 1982. Persons who have
expressed interest include the authors, Dr. Robert Serafin, NCAR-FOF,
Dr. Walter Frost, University of Tennessee, Dr. Ted Fujita, University
of Chicago, Dr. Richard Doviak, NSSL, Dr. Al Bedard, NOAA-WPL,
Dr. Fernando Caracena, NOAA-APCL, and Dr. Ron Alberty of NOAA - PROFS.
We see this program to be a comprehensive test of how wind shear affects
aircraft approach and departure operations, its detection, and its
warning.

REFERENCES

Bedard, A. J., Jr., F. H. Merrem, D. Simms, and M. M. Cairns, 1979: A Thunderstorm Gust-Front Detection System Part I. System Operation and Significant Case Studies Part II Statistical Results. Federal Aviation Administration Report No. FAA-RD-79-55, Washington, D.C., 130 pp.

Foy, W. H., 1979: Airborne Aids for Coping with Low-level Wind Shear. Federal Aviation Administration Report No. FAA-RD-79-117, Washington, D.C., 96 pp.

Frost, W., and B. Crosby, 1978: Investigations of Simulated Aircraft Flight Through Thunderstorm Outflows. NASA Contractor Report 3052, Washington, D.C., 110 pp.

Frost W., and K. R. Reddy, 1978: Investigation of Aircraft Landing in Variable Wind Fields. NASA Contractor Report 3073, Washington, D.C., 84 pp.

Frost, W., and B. Turkel, 1980: Pilot-Aircraft System Response to Wind Shear. Draft Interim Report, Contract NAS8-33458, FWG Associates, Inc., Tullahoma, TN, 80 pp.

Fujita, T. T., 1980: Downbursts and Microbursts--An Aviation Hazard. Preprints, 19th Conf. on Radar Meteor., Miami Beach Fla., Am. Meteor. Soc., Boston, Mass., 94-101.

Fujita, T. T., and F. Caracena, 1977: An Analysis of Three Weather-Related Aircraft Accidents. Bull. Am. Meteor. Soc., 11, 1165-1181.

Goff, R. C., 1976: Vertical Structure of Thunderstorm Outflows, Mon. Wea. Rev., 104, 1429-1440.

McCarthy, J., E. F. Blick, and R. R. Bensch, 1979: Jet Transport Performance in Thunderstorm Wind Shear Conditions. Final Contractor Report NASA CR-3207, Washington, D.C., 53 pp.

McCarthy, J., W. Frost, B. Turkel, R. J. Doviak, D. W. Camp, E. F. Blick, and K. L. Elmore, 1980a: An Airport Wind Shear Detection and Warning System Using Doppler Radar. Preprints, 19th Conf. on Radar Meteor., Miami Beach, Fla., Am. Meteor. Soc., Boston, Mass., 135-142.

McCarthy, J., K. L. Elmore, R. J. Doviak, and D. S. Zrnic, 1980b: Instrumented Aircraft Verification of Clear-Air Radar Detection of Low-Level Wind Shear. Preprints, 19th Conf. on Radar Meteor., Miami Beach, Fla., Am. Meteor. Soc., Boston, Mass., 143-149.

Offi, D. L., W. Lewis, and T. Lee, 1980: Wind Shear Detection with an Airport Surveillance Radar. Preprints, 19th Conf. on Radar Meteor., Miami Beach, Fla., Am. Meteor. Soc., Boston, Mass., 130-134.

Severe Environmental Storms and Mesoscale Experiment, 1978: SESAME 1979 Working Group Reports and Field Plans, NOAA Environmental Research Laboratories, Boulder, Colorado, 63 pp.

Severe Environmental Storms and Mesoscale Experiment, 1979a: SESAME 1979 Plans for Operations and Data Archival. NOAA Environmental Research Laboratories, Boulder, Colorado, 66 pp.

Severe Environmental Storms and Mesoscale Experiment, 1979b: SESAME 1979 Operations Summary. NOAA Environmental Research Laboratories, Boulder, Colorado, 253 pp.

Tinsley, H. G., F. G. Coons, L. W. Wood, 1978: Possible Near-Term Solutions to the Wind Shear Hazard. Preprints, Air Transportation Meeting, Boston, Mass., Society of Automative Engineers, Inc., Warrendale, Penn.

Wilson, J. W., R. E. Carbone, and R. J. Serafin, 1980: Detection and Display of Wind Shear and Turbulence. Preprints, 19th Conf. on Radar Meteor., Miami Beach, Fla., Am. Meteor. Soc., Boston, Mass., 150-156.

1. REPORT NO. NASA CR-3379	2. GOVERNMENT ACCESSION NO.	3. RECIPIENT'S CATALOG NO.
4. TITLE AND SUBTITLE An Airport Wind Shear Detection and Warning System Using Doppler Radar — A Feasibility Study		5. REPORT DATE January 1981
		6. PERFORMING ORGANIZATION CODE
7. AUTHOR(S) John McCarthy, Edward F. Blick, and Kim L. Elmore		8. PERFORMING ORGANIZATION REPORT #
9. PERFORMING ORGANIZATION NAME AND ADDRESS MCS, Inc. 239 Cedarbrook Road Boulder, Colorado 80302		10. WORK UNIT NO. M-326
		11. CONTRACT OR GRANT NO. NAS8-33458 (Sub. FWG 6-0510-1)
12. SPONSORING AGENCY NAME AND ADDRESS National Aeronautics and Space Administration Washington, D.C. 20546		13. TYPE OF REPORT & PERIOD COVERED Contractor Report
		14. SPONSORING AGENCY CODE

15. SUPPLEMENTARY NOTES

Marshall Technical Monitor: Dennis W. Camp

16. ABSTRACT
A feasibility study was conducted to determine whether ground-based Doppler radar could measure the wind along the path of an approaching aircraft with sufficient accuracy to predict aircraft performance. A severe storm research program, Severe Environmental Storms and Mesoscale Experiment (SESAME '79), provided the tools for this test, including two instrumented research aircraft, a Sabreliner and Queen Air from NCAR, a Doppler radar at NSSL, and an Air Force PAR unit for precision approaches to the Doppler radar. Forty-three PAR approaches were conducted, with 16 examined in detail. In each, Doppler-derived longitudinal winds were compared to aircraft-measured winds; in approximately 75 percent of the cases, the Doppler and aircraft winds were in acceptable agreement. In the remaining cases, errors may have been due to a lack of Doppler resolution, a lack of co-location of the two sampling volumes, the presence of eddy or vortex-like disturbances within the pulse volume, or the presence of point targets in antenna side lobes. It was further concluded that shrouding techniques would have reduced the side lobe problem. The work left little doubt that a ground-based Doppler radar operating in the optically clear air, would provide the appropriate longitudinal winds along an aircraft's intended flight path. The study also attempted to test whether, given the winds along the intended approach path taken immediately prior to the start of an approach, a fixed stick numerical simulation model could predict aircraft performance. Most of the test cases occurred in extremely weak wind shear conditions, and the resulting model calculation was unable to quantify precisely the aircraft performance, in terms of shear conditions. However, for the four approaches identified by an independent pilot assessment to be most severe, the model was more successful. This led to the conclusion that as the shear became more severe, the model's capability improved. However, this could not be verified in a convincing manner. Finally, some field results indicated that a high-performance jet transport (Sabreliner) was more adversely affected by shear than was a light piston transport (Queen Air), presumably operating in similar conditions.

17. KEY WORDS Aviation safety Wind shear Doppler radar Wind shear simulation Aircraft response	18. DISTRIBUTION STATEMENT Unclassified – Unlimited Subject Category 47

19. SECURITY CLASSIF. (of this report) Unclassified	20. SECURITY CLASSIF. (of this page) Unclassified	21. NO. OF PAGES 97	22. PRICE A05